Optical and Quantum Electronics **17** *(1985) 219–252*

Theoretical analysis of picosecond pulse development of passively mode-locked Nd–glass lasers*

A. PENZKOFER, F. GRAF
Naturwissenschaftliche Fakultät II – Physik, Universität Regensburg, 8400 Regensburg, Federal Republic of Germany

Received 20 December 1984; revised 22 February 1985

A realistic numerical theory of the temporal and spectral development of picosecond light pulses in a passively mode-locked Nd–glass laser is presented. The effects of the inhomogeneous gain profile of the active medium are considered. The calculations include the pulse development in the prelaser, the linear laser and the mode-locking region. In the mode-locking region two-photon absorption and self-phase modulation in the active medium as well as the bleaching dynamics of the mode-locking dye are included. The influence of self-phase modulation on the temporal pulse shape in active media of finite spectral gain width is analysed. The theoretical results are compared with the experimental findings.

1. Introduction

The development of picosecond light pulses in passively mode-locked Nd–glass lasers has been analysed theoretically in many papers ([1–18] and references cited therein). Analytical and numerical calculations were performed which gave a good qualitative understanding of the dynamics of picosecond pulse generation. These studies simplified the spectral development since they did not take account of the inhomogeneous gain profile of the active medium.

In recent experiments the picosecond pulse spectra obtained indicate the occurrence of spectral hole burning in the inhomogeneous gain profile of the active medium [19, 20]. A realistic numerical theory of the development of picosecond light pulses is presented here, including the effects of the inhomogeneous gain profile of the active medium. The effects of two-photon absorption in the laser medium are included in the calculations. The influence of self-phase modulation on the spectra is discussed. The numerical calculations apply to our passively mode-locked Nd–phosphate glass laser oscillator with the parameters listed in Table I.

In Section 2 a qualitative description of the generation of picosecond pulses in a mode-locked Nd–glass laser is given. It introduces the ideas on spectral hole burning and two-photon absorption.

The general equations for the pulse development are presented in Section 3. The inhomogeneous gain profile is included in the calculations. The statistics of light emission in the prelaser and linear laser phase is discussed.

The temporal and spectral development in the prelaser and linear laser phase is illustrated in Section 4. The initial conditions for the nonlinear laser region are presented.

In Section 5 the spectral development in the nonlinear phase is described. The effects of the inhomogeneous gain profile and of the two-photon absorption are included. A constant pulse duration is assumed in this analysis.

A theoretical discussion of the temporal pulse development is given in Section 6. The effects of the inhomogeneous gain profile are not included.

* This paper is dedicated to Professor W. Kaiser for his 60th birthday.

0306–8919/85 $03.00 + .12

TABLE I Parameters used in calculations (except changes as stated)

Resonator:
- front mirror: reflectivity, $R_1 = 0.997$; curvature, plane; part of contacted dye cell
- output mirror: reflectivity, $R_2 = 0.30$; curvature 3 m
- linear losses $T_l = 0.9$
- length $L_R = 1.50\,\text{m}$
- round-trip time $t_R = 2L_R/c = 10\,\text{ns}$

Active medium:
- type: Nd–phosphate glass rod Schott type LG703
- rod length: $l_R = 13\,\text{cm}$
- rod radius: $r = 0.4\,\text{cm}$
- pumped rod length: $l_A = 10\,\text{cm}$
- Nd^{3+}-concentration: $N_0 = 2.82 \times 10^{20}\,\text{cm}^{-3}$ [a]
- central lasing frequency: $\tilde{\nu}_0 = 9496\,\text{cm}^{-1}$ [a]
- fluorescence quantum efficiency: $\eta = 0.5$ [b]
- spontaneous lifetime: $\tau_{sp} = 240\,\mu\text{s}$ [a]
- inhomogeneous linewidth: $\Delta\nu_{IH} = 189\,\text{cm}^{-1}$, $\nu_G = 113\,\text{cm}^{-1}$ [a]
- homogeneous linewidth: $\Delta\nu_H = 20\,\text{cm}^{-1}$ [c]
- effective peak stimulated emission cross-section: $\bar{\sigma}_{em,0} = 4.1 \times 10^{-20}\,\text{cm}^2$ [a]
- peak stimulated emission cross-section: $\sigma_{em,0} = 2.74 \times 10^{-19}\,\text{cm}^2$ [d]
- cross-relaxation time $T_3 = 70\,\mu\text{s}$ [e] ($T_3 = \infty$ used in calculations)
- decay time of lower laser level $\tau_2 = 30\,\text{ns}$ [f] ($\tau_2 = 0$ used in calculations)
- two-photon absorption coefficient $\alpha^{(2)} = 4 \times 10^{-12}\,\text{cm W}^{-1}$ [g]
- nonlinear refractive index $n_2 = 1.2 \times 10^{-22}\,\text{m}^2\,\text{V}^{-2} = 1.08 \times 10^{-13}\,\text{esu}$ [h]

Flash lamps:
- active length $l_A = 10\,\text{cm}$
- total flash duration $\tau_{FL} = 1500\,\mu\text{s}$
- assumed temporal flash light shape $J(t)/J_0 = \sin(\pi t/\tau_{FL})$

Saturable absorber:
- type: Kodak No. 9860
- absorption recovery time $\tau_D = 7\,\text{ps}$ [i]
- isotropic absorption cross-section $\sigma_D = 3.7 \times 10^{-16}\,\text{cm}^2$ [j]
- small signal double-pass transmission $T_0 = 0.85^2 = 0.7225$

[a] Schott data sheet.
[b] [51].
[c] [32, 52–54].
[d] see Equation 8.
[e] [38] see also [20, 53].
[f] [34–37].
[g] [49].
[h] [81]; $n_2(\text{esu}) = 9 \times 10^8\, n_2(\text{SI})$.
[i] [45].
[j] [43–45].

The problem of self-phase modulation is discussed separately in Section 7. Influence of self-phase modulation on the spectral and temporal pulse shape is analysed.

In Section 8 the influence of self-focusing and optical dispersion is investigated.

Finally, in Section 9, the theoretical results are compared with experimental findings. Laser improvements such as spectral fixing with Fabry–Perot etalons and temporal pulse shortening by compression of natural mode-selection, by intensity optimization, by the combination of two saturable absorbers and by resonator switching to high saturable absorber concentration will be discussed.

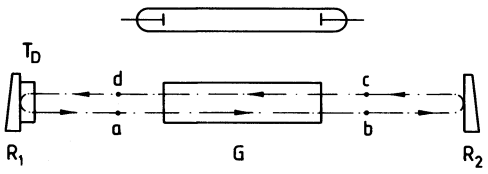

Figure 1 Laser oscillator.

2. Qualitative description of pulse development

The laser oscillator studied is depicted in Fig. 1. The resonator is formed by two mirrors with reflectivity R_1 and R_2. The active medium is inverted by firing a flash tube. The inversion of the active medium causes amplification of light with a gain G. Mode-locking is achieved with a saturable absorber contacted to a laser mirror (double-pass dye transmission T_D).

A level scheme of the active medium is shown in Fig. 2. The upper laser level 1 is populated by absorption of flash lamp light at higher lying levels and relaxation to the upper laser state. Level 1 is inhomogeneously broadened. The population distribution $N_1(\nu)$ is indicated. The upper laser level is depopulated by spontaneous and stimulated emission. The lower laser level 2 relaxes fast to the ground state 0.

The rate of population of the upper laser level $J(t)$ is depicted in Fig. 3a (experimentally, the half-width of pump pulse is approximately 700 μs). The accumulated number density of molecules N_1 is illustrated in Fig. 3b. Level 1 is depopulated by spontaneous emission (τ_{sp} = 240 μs for Schott phosphate glass LG703) and due to the laser action. Spontaneous emission is amplified and fed back to the active medium by the laser mirrors. Typical curves of loss L, gain G and net amplification $G_{net} = LG$ are plotted in Fig. 3c. The loss is given by

$$L = R_1 R_2 T_D T_1 T_{TPA} \tag{1}$$

R_1 and R_2 are the reflectivities of the laser mirrors. T_D is the double-pass dye transmission and T_1 summarizes additional linear resonator losses (mainly diffraction losses). T_{TPA} represents the transmission reduction by two-photon absorption in the active medium. Within the fluorescence linewidth of the active medium the losses are practically independent of frequency. The dye transmission T_D is equal to the small signal double-pass transmission T_0 except in the nonlinear region of the pulse development (Region III of Fig. 3c) where the intense pulses generated bleach the dye.

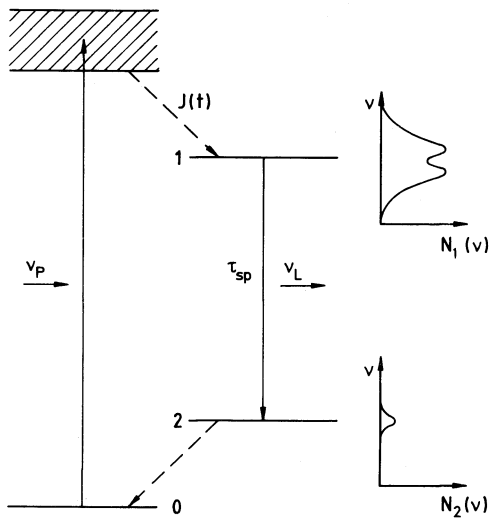

Figure 2 Level scheme of Nd^{3+}: glass active medium.

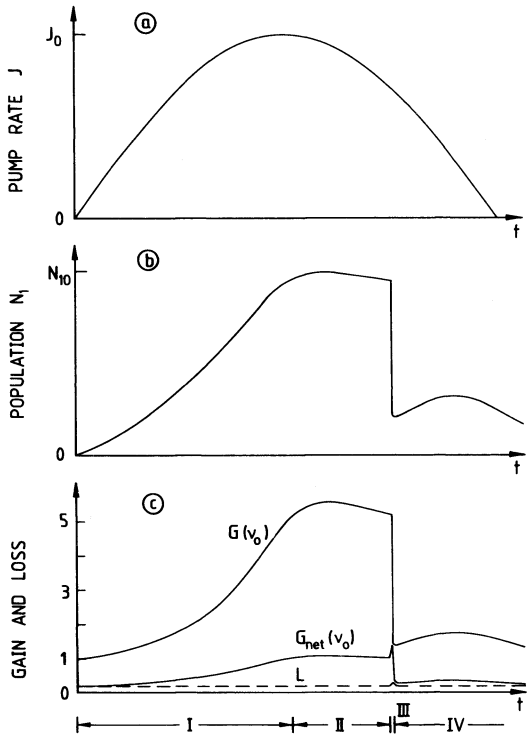

Figure 3 Upper laser level population (b) and laser gain (c) due to pulsed pump rate (a). I: prelaser region, II: linear laser range, III: nonlinear part, IV: post-laser region (schematic).

The gain $G(\nu)$ depends exponentially on the inversion $N_1(\nu)$ (see Equation 4 below). The gain $G(\nu_0)$ at the central frequency of spontaneous emission is shown by the upper curve of Fig. 3c. The net amplification $G_{net}(\nu) = LG(\nu)$ determines the spectral development of the laser light. The central component $G_{net}(\nu_0)$ is indicated by the middle curve of Fig. 3c. As long as $G_{net}(\nu_0) < 1$ the laser is below threshold (prelaser Region I). It follows the linear range, II, of laser action until the saturable absorber becomes partially bleached by the circulating laser emission.

In this nonlinear phase, III, the dye preferentially transmits the most intense spikes while its absorption remains high for weak noise pulses. The discriminating action of the absorber is responsible for the build-up of a train of single picosecond light pulses from the white noise laser light at the end of the linear phase. The generation of an intense picosecond pulse train declines the inversion and the gain. In the post-laser Region IV generally the net gain remains below the laser threshold $[G_{net}(\nu_0) < 1]$.

A more detailed picture of the frequency dependence of $G_{net}(\nu)$ with time is presented in Fig. 4. The upper part shows the temporal envelope of a generated pulse train. The prelaser region I and the linear region II are strongly compressed compared to the nonlinear range III. The set of pictures below the pulse train shows the spectral distribution of $G_{net}(\nu)$ (middle row) and the spectral shape of the laser light (bottom row) at the corresponding temporal regions. In the prelaser region (I, pictures a, a′) the loss L is given by the small signal loss $L_0(T_D = T_0)$ and $G_{net}(\nu_0) < 1$. A spectral narrowing of the emission sets in because of the spectral shape of $G_{net}(\nu)$. In the linear phase II the loss remains $L = L_0$ but the net gain grows to $G_{net}(\nu) > 1$ around the central frequency, ν_0. The spectral shape of the laser emission narrows further (natural mode selection, pictures b, b′). The early part of the nonlinear phase III is characterized by a reduction of the loss L for the most intense spikes in the oscillator. The net gain $G_{net}(\nu)$ increases and strong pulse amplification occurs (picture c, c′). The spectrally narrow peak of the generated light pulse interacts with inverted ions around the central frequency ν_0 within the homogeneous linewidth of the laser transition. The strong

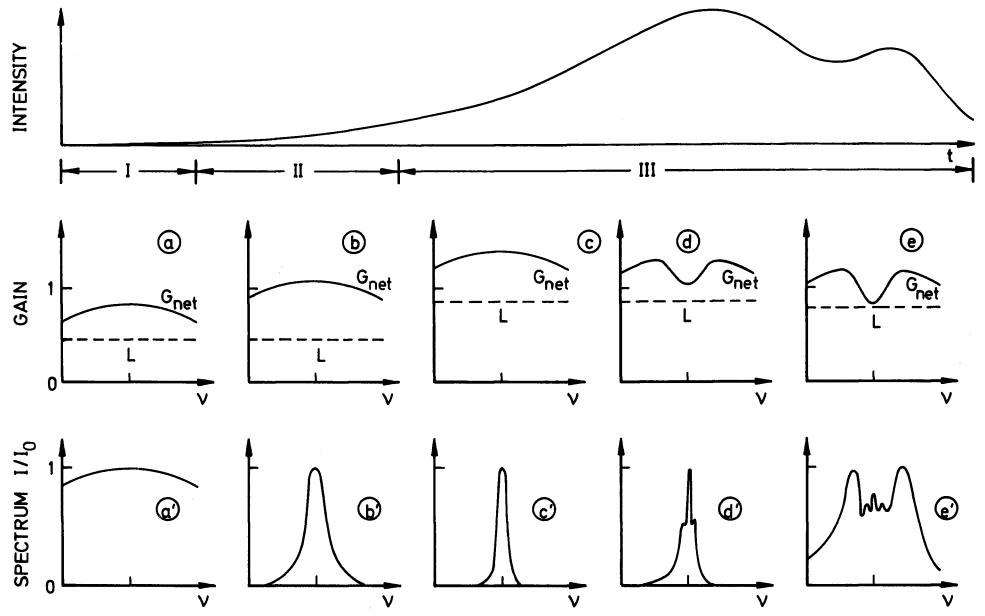

Figure 4 Spectral gain distribution and spectral pulse shapes along pulse train. a,a′: prelaser Region I; b,b′: linear laser Region II; c,c′: early part of nonlinear Region III; d,d′: pulse train maximum; e,e′: towards end of pulse train (schematic).

amplification depletes the central spectral region (pictures d, d′). The depletion causes a preferential amplification $G_{net}(\nu)$ in the wings of the laser pulse. Additionally the nonlinear interaction of the intense picosecond light pulses which are generated with the optical components inside the oscillator (mainly active medium) causes the onset of self-phase modulation [21–26] (spectral broadening and modulation, asymmetric spectral shape due to temporal asymmetric pulse shape). Beyond the pulse train maximum (the first maximum in the upper part of Fig. 4) the net gain at the central frequency drops below threshold $G_{net}(\nu_0) < 1$ while laser action remains in the wings (pictures, e, e′). Spectral peaks in the wings of the spectrum are generated by the prolonged laser action outside the central region. A second maximum in the pulse train envelope often builds up in the experiments before the pulse train ends.

To complete the description of picosecond pulse generation in a mode-locked Nd–glass laser the time dependences of intensity I, saturable absorber transmission T_D, and two-photon transmission T_{TPA} within a round trip time t_R ($t_R = 2L_R/c \simeq 10\,\text{ns}$, $L_R \simeq 1.5\,\text{m}$ resonator length) at various positions along the pulse train are depicted in Fig. 5.

During the prelaser and linear region the statistical spontaneous emission is equally amplified and remains white noise [27–30]. The transmission of the saturable dye is $T_D = T_0$ independent of time, and two-photon absorption in the active medium is not observable due to the low laser intensity ($I \lesssim 10^6\,\text{W cm}^{-2}$).

In the early part of the nonlinear region the most intense fluctuation reaches an intensity I comparable to the saturation intensity I_S of the mode-locking dye (the intensity scale is logarithmic in Fig. 5). This intense spike increases the dye transmission and is preferentially amplified (background suppression). The wings of the intense spike are more absorbed by the saturable dye than the peak leading to shortening of the pulse duration. Behind the most intense spike the dye transmission relaxes to the small signal transmission T_0 with the recovery time τ_D ($\tau_D \simeq 7\,\text{ps}$ for Kodak dye No. 9860). The most intense spike begins to suffer two-photon absorption in the active medium.

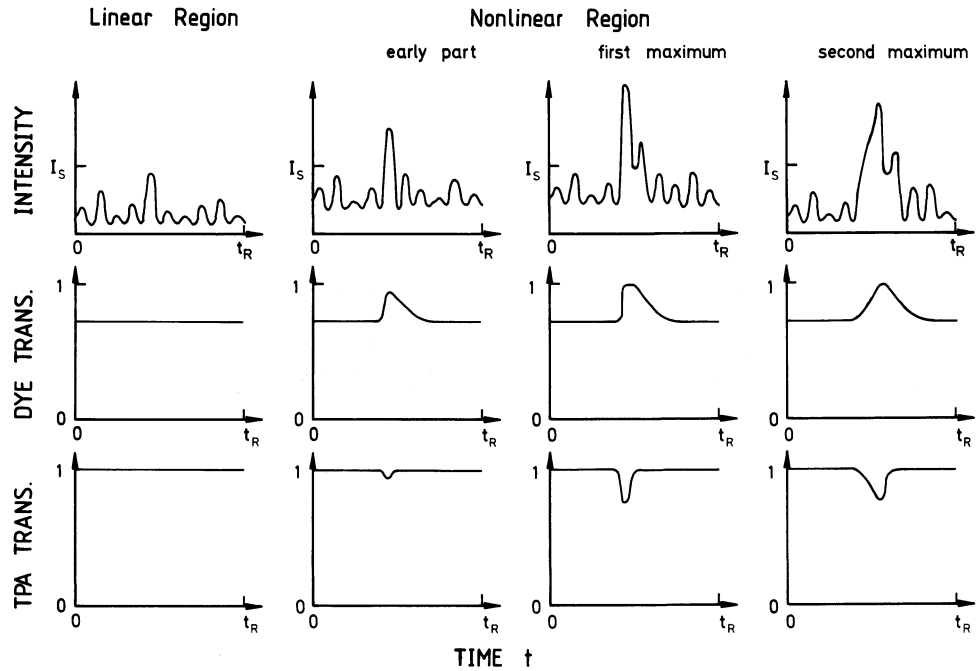

Figure 5 Laser emission within round-trip time together with dye transmission and two-photon transmission along pulse train (schematic).

Around the first pulse train maximum an intense picosecond pulse circulates in the resonator and bleaches the dye completely. Within the opening time of the absorber the trailing part of the intense pulse and additional spike radiation are strongly amplified, preferentially in the spectral wings (see Fig. 4). The two-photon absorption for the intense picosecond pulse has increased. The loss by two-photon absorption limits the peak intensity of the most intense pulse and increases its pulse duration. Towards the end of the pulse train and in the case of the occurrence of a second pulse train maximum the leading part of the picosecond pulse has decreased and the trailing pulse region has grown up in intensity to a peak value. The spectral emission has shifted to the wings (Fig. 4). Finally all pulses fade away since the inversion is depleted.

3. General equations

Spontaneous emission occurs in the laser resonator (in statistical fashion) and also amplification of radiation which is fed back to the active medium. The upper laser level 1 is inhomogeneously broadened and the population is spectrally distributed according to

$$N_1(\nu, t) = N_1(t) g_{IH}(\nu - \nu_0) \tag{2}$$

$g_{IH}(\nu - \nu_0)$ describes the normalized spectral distribution of the upper laser levels with respect to the corresponding frequency positions of the lower laser levels (ν is frequency separation between upper and lower level of a specific Nd^{3+} ion). ν_0 is the central laser transition frequency. We assume a gaussian distribution:

$$g_{IH}(\nu - \nu_0) = \pi^{-1/2} \nu_G^{-1} \exp\left[-(\nu - \nu_0)^2/\nu_G^2\right] \tag{3}$$

ν_G is the half $1/e$-width of the inhomogeneous emission profile.

The spectrally resolved amplification of the active medium per round trip is

$$G(\nu, t) = \exp\left[2 \int_0^{l_A} \alpha_{em}(\nu, t, z)\, dz\right] \tag{4}$$

l_A is the length of the active medium. The gain coefficient $\alpha_{em}(\nu)$ is given by

$$\alpha_{em}(\nu, t, z) = [N_1(t, z) - N_2(t, z)] \int_{-\infty}^{\infty} g_{IH}(\bar{\nu} - \nu_0)\sigma_{em}(\nu - \bar{\nu})\,d\bar{\nu} \tag{5}$$

$\sigma_{em}(\nu - \bar{\nu})$ is the stimulated emission cross-section at light frequency ν for an ion with transition frequency $\bar{\nu}$. The spectral shape of $\sigma_{em}(\nu - \bar{\nu})$ reflects the homogeneous broadening of the emission from level 1 to 2. It is given by

$$\sigma_{em}(\nu - \bar{\nu}) = \sigma_{em} g_H(\nu - \bar{\nu}) = \sigma_{em,0}\tilde{g}_H(\nu - \bar{\nu}) \tag{6}$$

with $\int_{-\infty}^{\infty} g_H(\nu - \bar{\nu})\,d\nu = 1$ and $\tilde{g}_H(0) = 1$. σ_{em} is the integrated emission cross-section and $\sigma_{em,0}$ is the peak stimulated emission cross-section. The homogeneous distribution is given by

$$g_H(\nu - \bar{\nu}) = \frac{\Delta\nu_H}{2\pi} \frac{1}{(\nu - \bar{\nu})^2 + (\Delta\nu_H/2)^2} \tag{7a}$$

and

$$\tilde{g}_H(\nu - \bar{\nu}) = \pi \frac{\Delta\nu_H}{2} g_H(\nu - \bar{\nu}) \tag{7b}$$

The stimulated emission cross-sections reported in the literature [31–33] are defined in another way since no distinction is made between inhomogeneous and homogeneous broadening. The relation between the published effective peak emission cross-section $\bar{\sigma}_{em,0}$ and $\sigma_{em,0}$ is given by Equation 8

$$\bar{\sigma}_{em,0} = \frac{\alpha_{em}(\nu_0, t)}{N_1(t)} = \sigma_{em,0} \frac{\Delta\nu_H^2}{4\pi^{1/2}\nu_G} \int_{-\infty}^{\infty} \frac{\exp[-(\nu/\nu_G)^2]}{\nu^2 + (\Delta\nu_H/2)^2}\,d\nu \tag{8}$$

With the data of Table I, $\sigma_{em,0} = 6.7\bar{\sigma}_{em,0}$. The net amplification of light per round trip is

$$G_{net}(\nu, t) = G(\nu, t)L \tag{9}$$

where the loss factor L per round trip is given by Equation 1. The average spontaneously emitted temporal power is

$$\bar{P}_{sp}(t) = \frac{h\nu_0\eta}{\tau_{sp}} VN_1(t) \tag{10}$$

η is the fluorescence quantum efficiency and τ_{sp} the spontaneous lifetime of the upper laser level. $V = \pi r_A^2 l_A$ is the volume of the active medium and r_A is the rod radius. The average spontaneous intensity that hits the laser mirrors is fed back to the active medium and will be amplified. Its value is found by dividing the total spontaneous power by the surface $A = 4\pi(L_R/2)^2 = \pi L_R^2$ of a sphere of radius $L_R/2$ (L_R separation of laser mirrors):

$$\bar{I}_{sp}(t) = \frac{h\nu_0\eta}{\tau_{sp}} \frac{r_A^2 l_A}{L_R^2} N_1(t) \tag{11}$$

The average temporal–spectral intensity distribution of spontaneous emission is $\bar{I}_{sp}(\nu, t) = I_{sp}(t)g_{IH}(\nu - \nu_0)$ (dimension $W\,cm^{-2}\,s$). Applying Equations 11 and 2 one finds

$$\bar{I}_{sp}(\nu, t) = \frac{h\nu\eta}{\tau_{sp}} \frac{r_A^2 l_A}{L_R^2} N_1(\nu, t) \tag{12}$$

The fluorescence contribution to the spectral intensity per round trip time in the oscillator $t_R = 2L_R/c$ is $\Delta\bar{I}_{sp}(\nu) = \int_{t-t_R}^{t} \bar{I}_{sp}(\nu, t)\,dt$ (dimension $J\,cm^{-2}\,s$). The relation between spectral intensity and temporal intensity is $\int I(\nu)\,d\nu = \int I(t)\,dt$.

The spectral and temporal dynamics of the laser are governed by the following rate equations for

the level populations

$$\frac{dN_1(\nu, t, z)}{dt} = J(\nu, t) - \frac{N_1(\nu, t)}{\tau_{sp}} - \frac{N_1(\nu, t) - N_2(\nu, t)}{h\nu} \times \int I(\bar{\nu}, t, z)\sigma_{em}(\nu - \bar{\nu})\,d\bar{\nu} - \frac{N_1(\nu, t) - N_1(t)g_{IH}(\nu - \nu_0)}{T_3} \tag{13}$$

$$\frac{dN_2(\nu, t, z)}{dt} = \frac{N_1(\nu, t, z)}{\tau_{sp}} + \frac{N_1(\nu, t, z) - N_2(\nu, t, z)}{h\nu} \times \int I(\bar{\nu}, t, z)\sigma_{em}(\nu - \bar{\nu})\,d\bar{\nu} - \frac{N_2(\nu, t, z)}{\tau_2} - \frac{N_2(\nu, t, z) - N_2(t, z)g_{IH}(\nu - \nu_0)}{T_3} \tag{14}$$

and by a gain–loss equation for the intensities per round trip

$$I(\nu, t) = I(\nu, t - t_R)G(\nu, t - t_R)L + I_{sp}(\nu, t - t_R)(1 + L) \tag{15}$$

The first term of Equation 13 describes the filling of the upper laser level by the pump process. The second term represents the level depopulation by spontaneous emission and the third term takes care of stimulated emission. The last term is due to spectral cross-relaxation. T_3 is the spectral cross-relaxation time.

In Equation 14 the first and second term describe the population of the lower laser level by spontaneous and stimulated emission, respectively. The third term is responsible for the relaxation to the ground state 0 with time constant τ_2. The last term considers spectral cross-relaxation.

Equation 15 relates the light intensity in the resonator at time t to the intensity of the preceding transit at time $t - t_R$. The first term gives the net gain (G gain, L loss) while the second term adds the contribution of the instantaneous spontaneous emission.

The relation between the instantaneous spontaneous emission $I_{sp}(\nu, t)$ and the average spontaneous emission $\bar{I}_{sp}(\nu, t)$ is governed by statistical laws of white light emission (gaussian light). Since laser emission is initiated by spontaneous emission (Equation 15), the white light statistics remain valid in the linear amplification region (as long as $L = L_0 =$ constant). Only parameters of the white light emission change due to the spectral dependence of light amplification (natural mode selection, see below). In the nonlinear laser regime the intensity dependence of the loss factor $L = L(I)$ causes preferential amplification of intense flunctuations and the statistics changes to the formation of picosecond pulse trains (passive mode-locking). We do not completely discuss the problems of the statistics [4, 7–11, 27–30] but rather summarize some results which we need in the following sections.

The mean duration of an emission fluctuation (gaussian shape) of spatial width $\Delta\nu$ (FWHM) is given by the Heisenberg uncertainty principle to be

$$\Delta t = \frac{0.44}{\Delta\nu} \simeq \frac{0.5}{\Delta\nu} \tag{16}$$

The number of pulses within a resonator round trip time $t_R = 2L_R/c$ is expected to be

$$m \simeq \frac{t_R}{2\Delta t} \simeq t_R\Delta\nu = \frac{2L_R\Delta\nu}{c} \tag{17}$$

The peak intensity distribution of the spikes within a round trip time is determined by a gaussian distribution. The peak intensity distribution function is given by

$$w(I) = \frac{1}{\langle I\rangle}\exp(-I/\langle I\rangle) \tag{18}$$

where $\langle I \rangle$ is the average peak intensity of the pulses ($\int w(I)\,dI = 1$). The number of fluctuations μ with $I \geqslant I_0$ is found by

$$\mu = m \int_{I_0}^{\infty} w(I)\,dI = m \exp(-I_0/\langle I \rangle) \tag{19}$$

By setting $\mu = 1$ we find that one pulse has a peak intensity $I_{p,1}$ higher than the corresponding $I_{0,1}$ value of Equation 19, i.e.

$$I_{p,1} \geqslant I_{0,1} = \langle I \rangle \ln(m) \tag{20}$$

Similarly the average peak intensity of the ith most intense pulse is

$$I_{p,i} = \frac{\langle I \rangle}{2}\left[\ln\left(\frac{m}{i-1}\right) + \ln\left(\frac{m}{i}\right)\right] \tag{21}$$

For the Nd–phosphate glass laser (data see Table I) the statistics applied to the spontaneous emission gives: (i) an average spike duration $\Delta t \simeq 8 \times 10^{-14}$ s, (ii) an average number of spikes $m \simeq 57\,000$, and (iii) a peak intensity of most intense spike $I_{p,1} \geqslant I_{0,1} \simeq 11\langle I \rangle$.

The laser emission remains gaussian noise until the end of the linear phase. The spike parameters change due to the natural mode selection. For $\Delta\tilde{\nu} = \Delta\nu/c \simeq 2\,\mathrm{cm}^{-1}$ at the end of the linear phase (see Section 4) the characteristic parameters of the emission are $\Delta t \simeq 9$ ps, $m \simeq 556$, and $I_{0,1} \simeq 6.5\langle I \rangle$. These data are used as initial conditions for the calculation of the temporal pulse development in the nonlinear phase of pulse generation (see Section 7).

Equations 1 to 21 describe the temporal and spectral development of laser pulses. The effect of self-phase modulation is not included. For the prelaser and linear laser region the equations will be simplified in the following section. In the nonlinear region the complete equation system has to be solved (Section 5).

4. Temporal and spectral development in the prelaser and linear laser phase

In the prelaser and linear laser phase the general rate Equations 13 to 15 are simplified by three assumptions:

1. The population of the lower laser level is neglected ($N_1 - N_2 \simeq N_1$) since the depopulation time τ_2 of the lower laser level is very fast [34–37].

2. The spectral shape of the inhomogeneous level population is assumed to remain unchanged, i.e. $N_1(\nu, t) = N_1(t) g_{IH}(\nu - \nu_0)$. This condition is valid as long as depletion of inversion by stimulated emission is negligible. It is fulfilled in the prelaser and linear laser region. It would be correct for all times in the case of purely homogeneously broadened laser transitions. It breaks down for inhomogeneously broadened transitions (as in our case) in the nonlinear laser region where depletion of inversion occurs. It even breaks down for the free running laser when relaxation spike duration Δt_{RS} becomes shorter than the spectral cross relaxation time T_3 [20] ($T_3 \simeq 70\,\mu$s [38]).

3. The intensity distribution within the round-trip time t_R is averaged and only the growth of the average intensity $\bar{I}(t)$ and the average spectral–temporal intensity $\bar{I}(\nu, t)$ is considered, i.e.

$$\bar{I}(t) = \frac{1}{t_R}\int_{t-t_R}^{t} I(t')\,dt' \quad \text{and} \quad \bar{I}(\nu, t) = \frac{1}{t_R}\int_{t-t_R}^{t} I(\nu, t')\,dt'.$$

This averaging is possible since in the prelaser and linear laser region the net gain is independent of the statistically varying spike intensities.

Considering the total population of the upper laser level integration of Equation 13 leads to

$$\frac{dN_1(t)}{dt} = J(t) - \frac{N_1(t)}{\tau_{sp}} - \frac{N_1(t)\sigma_{em,0}}{h\nu_0}\int_{-\infty}^{\infty} \bar{I}(\nu, t)\left[\int_{-\infty}^{\infty} g_{IH}(\tilde{\nu} - \nu_0)\tilde{g}_H(\tilde{\nu} - \nu)\,d\tilde{\nu}\right]d\nu \tag{22}$$

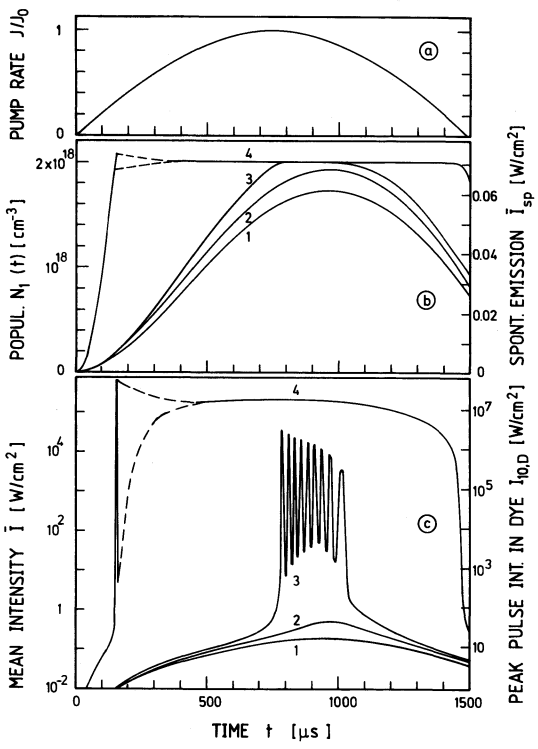

Figure 6 (a) Population rate of upper laser level. (b) Upper laser level population $N_1(t)$ for different pump rates J_0 of free-running laser ($T_D = T_0$). (1) $J_0 = 8 \times 10^{21}\,\mathrm{cm^{-3}s^{-1}}$, (2) $J_0 = 9 \times 10^{21}\,\mathrm{cm^{-3}s^{-1}}$, (3) $J_0 = 10^{22}\,\mathrm{cm^{-3}s^{-1}}$, (4) $J_0 = 10^{23}\,\mathrm{cm^{-3}s^{-1}}$. The mean spontaneous emission intensity scale (Equation 11) is shown at the right ordinate. (c) Mean laser intensity (averaged over round trip time t_R) of free-running laser. Same pump rate as in (b). Peak intensity of most intense pulse within round trip time at the position of the dye cell is indicated by the right ordinate.

The average temporal–spectral intensity is found from Equation 15:

$$\bar{I}(\nu, t) = \bar{I}(\nu, t - t_R)G(\nu, t - t_R)L_0 + \bar{I}_{sp}(\nu, t - t_R)(1 + L_0) \tag{23}$$

with

$$G(\nu, t) = \exp\left[2l_A N_1(t)\sigma_{em,0}\int_{-\infty}^{\infty} g_{IH}(\bar{\nu} - \nu_0)\tilde{g}_H(\nu - \bar{\nu})\,d\bar{\nu}\right] \tag{24}$$

and

$$\bar{I}_{sp}(\nu, t) = \frac{h\nu_0\eta}{\tau_{sp}}\frac{r_A^2 l_A}{L_R^2} N_1(t) g_{IH}(\nu - \nu_0) \tag{25}$$

The average laser intensity at time t is

$$\bar{I}(t) = \int_{-\infty}^{\infty} \bar{I}(\nu, t)\,d\nu \tag{26}$$

The results of the calculations by use of Equations 22 to 26 are depicted in Figs. 6 to 8. Parameters of Table I are used. Fig. 6a indicates the temporal shape of the pump rate $J(t) = J_0 \sin(\pi t/\tau_{FL})$. The population of the upper laser level for four different pump rates is shown in Fig. 6b. Since the spontaneous emission is proportional to the population of the upper laser level (Equation 11), the curves also represent the spontaneous intensity (right ordinate). Curves 1 and 2 belong to the prelaser situation, with the pump rate below the threshold pump rate. For Curve 3 the laser threshold is reached at $t \simeq 780\,\mu s$ near the top of the pump rate curve. The threshold level population is $2 \times 10^{18}\,\mathrm{cm^{-3}}$. In the case of Curve 4 the peak pump rate J_0 is about a factor of ten above threshold. The threshold inversion is reached early. The upper laser level population oscillates slightly around the threshold population in a damped version. The average level population is independent of the pump rate. Fig. 6c depicts the average temporal laser intensity $\bar{I}(t)$ as a function of time (Equation 26) for the same pump rates as in Fig. 6b. Below the threshold (Curves 1 and 2)

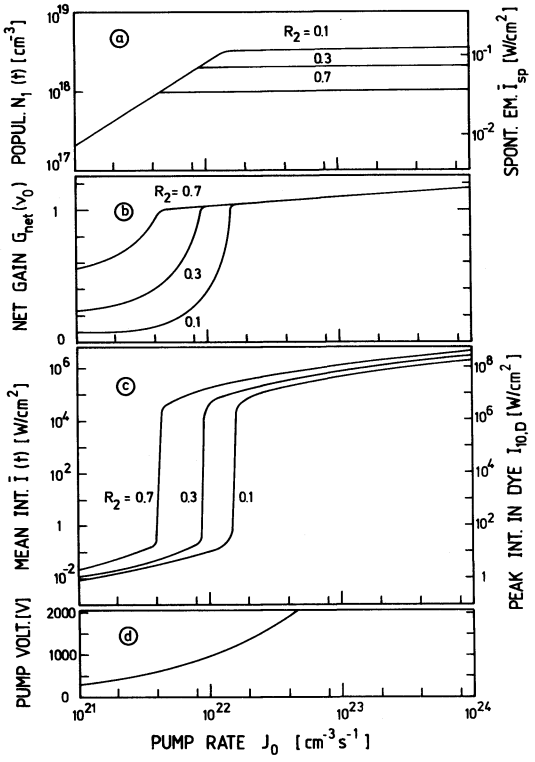

Figure 7 Upper laser level population (a), net laser gain (b), mean laser intensity (c) and necessary pump voltage (d) versus peak pump rate J_0 (Fig. 6a). Laser is free-running. Curves for three different output mirror reflectivities are presented. Intensities of spontaneous emission (a) and of peak fluctuation intensity in contacted dye cell (c) are indicated.

the intensity of the emission is only slightly higher than the spontaneous emission of Fig. 6b. As the laser threshold is approached the laser intensity increases rapidly and oscillates around a mean value (Curve 3). These relaxation spikes are damped. Towards the end of the pump pulse the light emission decreases since the pump rate falls below the threshold rate. Curve 4 indicates that the spike height and spike modulation grow with pump rate.

The average intensity $\bar{I}(t)$ was calculated for a position in the laser rod. The average intensity in the mode-locking dye depends on the resonator geometry and dye cell position. In our case the dye cell is contacted to the 100% plane front mirror (cell thickness 0.1 mm) and the output mirror has a curvature of 3 m. Superposition of the reflected pulse with itself increases the intensity by a factor of 3 [39]. The rod is arranged under Brewster's angle near to the output mirror (Brewster angle reduces intensity inside rod by about a factor of 1.5 due to a change in beam cross-section). The total increase in intensity is $f \simeq 6.5$. The peak intensity of the most intense pulse of the amplified white noise is again a factor of 7.1 higher than the averge peak intensity $\langle I \rangle$ which itself is a factor a two higher than the mean intensity $\bar{I}$ averaged over the round-trip time. The peak intensity $I_{p,1}$, of the most intense fluctuation in the dye cell is about a factor of 90 higher than the mean intensity $\bar{I}$ in the laser rod. Its value is indicated by the right-hand ordinate of Fig. 6c.

Figs. 7a, b and c depict the peak values of upper laser level population $N_1(t)$, of net gain at the central laser frequency $G_{net}(\nu_0)$, and of mean laser intensity $\bar{I}(t)$ versus pump rate, respectively. The curves are calculated for various reflectivities R_2 of the output mirror. In Fig. 7d the flash lamp pump voltage necessary to generate the pump rate is plotted (capacity of the power supply is 500 μF, with an assumed efficiency of 0.05). Fig. 7a indicates that the population level increases linearly with pump rate until the pump threshold is reached. Then the population remains constant against pump rate. A small mirror reflectivity requires higher threshold populations. The net gain $G_{net}(\nu_0)$ increases with pump rate in the prelaser region. Above laser threshold the steady state value is $G_{net}(\nu_0) = 1$. $G_{net}(\nu_0)$ rises slightly with pump rate only due to relaxation oscillations.

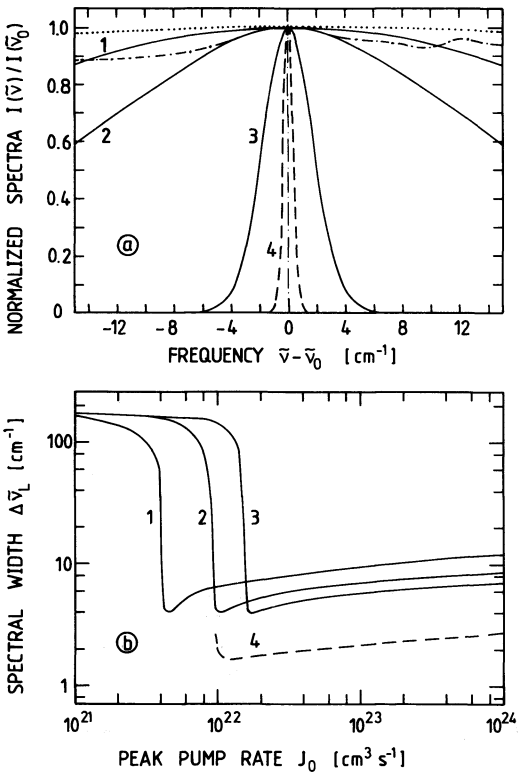

Figure 8 (a) Normalized spectra of free-running laser at first spike maximum. Dotted curve: assumed gaussian distribution of fluorescence spectrum for spectra 1 to 3. Dash-dotted curve: measured shape of fluorescence spectrum of Nd-glass laser rod LG703 used for calculation of spectrum 4. Curve 1: pump rate $J_0 = 8 \times 10^{21}\,\mathrm{cm^{-3}\,s^{-1}}$, time $t = 900\,\mu\mathrm{s}$; Curve 2: $J_0 = 9 \times 10^{21}\,\mathrm{cm^{-3}\,s^{-1}}$, $t = 900\,\mu\mathrm{s}$. Curves 3 and 4: $J_0 = 10^{22}\,\mathrm{cm^{-3}\,s^{-1}}$, $t = 780\,\mu\mathrm{s}$. Output mirror reflectivity $R_2 = 0.3$. (b) Spectral half-widths (FWHM) at first spike position versus pump rate. Curve 1: $R_2 = 0.7$; 2: $R_2 = 0.3$; 3: $R_2 = 0.1$; 4: $R_2 = 0.3$. Curves 1–3 belong to gaussian fluorescence shape (dotted curve above). Curve 4 belongs to experimental fluorescence spectrum (dash-dotted curve above).

The mean intensity of the emitted radiation $\bar{I}(t)$ is slightly above the spontaneous emission intensity at low pump rate, but rises strongly when the laser threshold is approached. Above the threshold the laser intensity increases proportional to the pump rate [40].

The spectral dependence of the (free-running) laser is illustrated in Fig. 8 [$I(\nu) = \bar{I}(\nu, t)t_R$]. The upper picture (Fig. 8a) shows normalized spectra. The dotted curve represents the fluorescence spectrum at low pump rate [$I_{sp}(\nu) \propto \int g_{IH}(\bar{\nu} - \nu_0) g_H(\bar{\nu} - \nu)\,\mathrm{d}\bar{\nu}$]. Curves 1 and 2 are just below threshold. They belong to $R_2 = 0.3$ and pump rates $J_0 = 8 \times 10^{21}$ and $9 \times 10^{21}\,\mathrm{cm^{-3}\,s^{-1}}$ at $t = 900\,\mu\mathrm{s}$ (see Fig. 6), respectively. They are slightly narrowed. Curve 3 represents the spectrum at the first spike maximum slightly above laser threshold ($J_0 = 10^{22}\,\mathrm{cm^{-3}\,s^{-1}}$, $R_2 = 0.3$, $t \simeq 780\,\mu\mathrm{s}$, see Fig. 6). The spectrum is narrowed by the spectral shape of the inversion profile (natural mode selection). The experimentally obtained fluorescence spectrum of the laser rod has the spectral shape of the dash-dotted curve. The spectral shape of Curve 4 belongs to this spectral distribution at the laser threshold. The experimentally observed spectrum of the free-running laser has a spectral width of $\Delta\tilde{\nu} = 2\,\mathrm{cm^{-1}}$ in agreement with Curve 4.

The dependence of the halfwidth of the first spike of emission on pump rate is plotted in Fig. 8b for the three mirror reflectivities $R_2 = 0.7$, 0.3 and 0.1. The halfwidth is greatly reduced when the pump threshold is approached. At higher pump rates the spectral width of the first spike slightly increases due to the fast transit through the prelaser region. The solid Curves 1 to 3 are calculated for the theoretical spectral fluorescence shape of the dotted curve of Fig. 8a while the dashed Curve 4 is calculated from the experimental fluorescence shape of the dash-dotted curve of Fig. 8a ($R_2 = 0.3$). The spectral narrowing (natural mode selection) broadens the temporal width of the amplified light fluctuations (Equation 16).

The peak spike intensity in the saturable absorber cell has to be high enough to start the mode-locking action by beginning to bleach the dye. A characteristic parameter of the absorber is the saturation intensity I_S. It is defined as the laser intensity where the absorption coefficient is

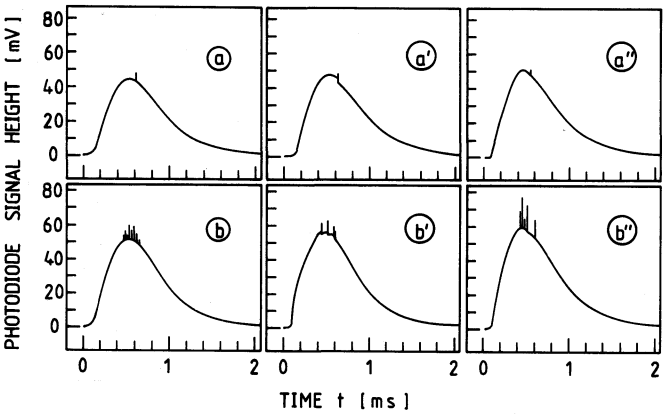

Figure 9 Off-axis light emission of laser oscillator. (a) Free-running laser at threshold. (b) Free-running laser with pump voltage 10 percent above threshold. (a′) Mode-locked laser at threshold; dye Kodak No. 9860. (b′) Mode-locked laser above threshold; dye No. 9860. (a″) Dye No. 5 in resonator, laser at spiking threshold. (b″) Dye No. 5 in resonator, laser at mode-locking threshold.

reduced to half its small signal value under steady state conditions. When the absorber is described by a three-level system with fast intermediate state, its value is given by [41, 42]

$$I_S = \frac{h\nu_L}{\sigma_D \tau_D} \tag{27}$$

σ_D is the orientation-averaged absorption cross-section and τ_D the absorption recovery time of the saturable dye. Slight bleaching necessary to initiate mode-locking starts already at intensities a factor of 50 below the saturation intensity (see Fig. 10a). The saturation intensities of two experimentally often used mode-locking dyes No. 9860 (Kodak) and No. 5 (Kodak and Lambda Physik) are 7.3×10^7 and $2.3 \times 10^8\,\mathrm{W\,cm^{-2}}$, respectively (No. 9860: $\sigma_D = 3.7 \times 10^{-16}\,\mathrm{cm^2}$ [43–45], $\tau_D = 7\,\mathrm{ps}$ [45]; No. 5: $\sigma_D = 3.0 \times 10^{-16}\,\mathrm{cm^2}$ [46], $\tau_D = 2.7\,\mathrm{ps}$ [45]).

In the case of saturable absorber No. 9860 the intensity of the peak fluctuation of laser light at pump rate threshold ($I_{p,l,D} \simeq 2.5 \times 10^6\,\mathrm{W\,cm^{-2}}$) is strong enough to initiate mode-locking. This behaviour was confirmed experimentally by the following measurements.

1. The threshold flash lamp pump voltage for the free-running laser without absorber and for the mode-locked laser with absorber remained unchanged as long as the resonator had the same linear losses (for a free running laser a neutral density filter was inserted to take care of dye loss).

2. The fluorescence light and laser relaxation spikes were registered with a fast photodiode in an off-axis position. The measured signals are depicted in Fig. 9. For the free-running laser without absorber (Figs. 9a and b) spiking was observed. At threshold (Fig. 9a) a single spike appears slightly behind the fluorescence maximum. Already, slightly above threshold, (pump voltage 10% above threshold), irregular spiking sets in (chaos formation [47]) at the rising part of the fluorescence emission (Fig. 7b). With the mode-locking dye No. 9860 in the resonator only one spike at the pump threshold position was registered (Fig. 9a′) and a train of picosecond pulses was detected. The fluorescence emission breaks in at the spike position due to depletion of inversion by the picosecond pulse train formation. Above laser threshold (Fig. 9b′) more spikes are formed and the mode-locking action is achieved at one or several spikes (one or more break-ins). The inhomogeneous spectral distribution allows the occurrence of several spikes above threshold even if mode-locking is achieved only once. In the case of picosecond pulse generation with mode-locking dye No. 5 [13, 46, 48] the free-running laser threshold and the mode-locking threshold did not coincide. Using the pump rates of threshold mode-locking with dye A9860 only spiking was observed (Fig. 9a″). The spike intensity becomes insufficient to initiate mode-locking because of the increased saturation intensity. The pump rate power had to be increased in order to obtain mode-locking action (Fig. 9b″). The laser threshold changed from shot to shot. At a fixed pump rate, very often no mode-locking was achieved. A folded cavity geometry with the beam focusing into the saturable

absorber cell was employed [13], in order to achieve mode-locking. Mixing of dye No. 9860 and No. 5 was applied [44, 46] to use the advantages of low mode-locking threshold of dye No. 9860 and of the short recovery time of dye No. 5.

5. Spectral development in the nonlinear phase

In the nonlinear phase the most intense fluctuations increase the dye transmission and are preferentially amplified. The general system Equations 13 to 15 have to be solved. In the following we discuss the effects of dye bleaching, gain saturation, spectral hole burning and two-photon absorption on the pulse train development. We assume a constant pulse duration along the pulse train in the nonlinear region as is approximately observed experimentally. A theoretical discussion of the temporal pulse development is given in the next section. The problem of self-phase modulation will be analysed separately in Section 7.

The calculation of the pulse development in the nonlinear phase starts from the results of level population and pulse spectrum at the end of the linear phase. The pulse development changes over to the non-linear region near the peak of the first relaxation spike where the average temporal pulse intensity in the active medium is about $3 \times 10^4\,\mathrm{W\,cm^{-2}}$ and the peak intensity of the most intense circulating fluctuation within the round trip time in the saturable absorber is about $2.5 \times 10^6\,\mathrm{W\,cm^{-2}}$ (see Fig. 6).

After j_0 round trips in the prelaser and linear laser region ($j_0 \simeq 75\,000$) the initial conditions for the nonlinear phase are:

1. The upper laser level population is given by

$$N_1(\nu, j_0, k) = N_1(t = j_0 t_R) g_{1H}(\nu - \nu_0) \tag{28}$$

k represents the spatial position $z = k\Delta z$ in the active medium ($\Delta z = l_A/K$, K number of segments into which the active medium is divided). $N_1(\nu, j_0, k)$ is equal to $N_{1,cd}(\nu, j_0, k)$ in Equation 33 (see Fig. 1).

2. The population of the lower laser level is neglected in order to save computer time. It is justified by the fast relaxation of the lower laser level to the ground state [34–36].

3. The average temporal–spectral pulse intensity in the active medium at the beginning of the nonlinear phase is

$$\bar{I}(\nu, t, j_0, k = 0) = \bar{I}(\nu, t, j_0) = I(\nu, j_0)/t_R \tag{29}$$

where $\bar{I}(\nu, t, j_0)$ is given by Equation 23. $I(\nu, j_0)$ is the spectral pulse intensity in the active medium within one round trip. The spectral shape of Curve 3 in Fig. 8 is used in the calculations. In the resonator within a round trip time m pulses are circulating with temporal–spectral intensity distribution $I_i(\nu, t, j, k)$ and duration Δt. The initial value of the ith most intense pulse is

$$I_i(\nu, t, j_0, k = 0) = \beta_i \bar{I}(\nu, t, j_0, k = 0) \tag{30}$$

The spectral intensity of each pulse is

$$I_i(\nu, j, k) = \int I_i(\nu, t, j, k)\,\mathrm{d}t \simeq I_i(\nu, t, j, k)\,\Delta t \tag{31}$$

where β_i is the ratio of peak pulse height of ith highest pulse to average peak pulse height ($\beta_i \simeq \frac{1}{2}\{\ln[m/(i-1)] + \ln(m/i)\}$, see Equation 21).

In our calculations we simplify the temporal–spectral distribution by considering explicitly only the two most intense pulses (subscripts 1, 2), two pulse packets following immediately the most intense pulses (subscripts 5, 6) and three clusters of pulses (subscripts 3, 4 and 7). The selected β-values are

$$\beta_1 = [\ln(2m) + \ln(m)]/2 \tag{32a}$$

$$\beta_2 = [\ln(m) + \ln(m/2)]/2 \tag{32b}$$

$$\beta_3 = [\ln(m/2) + \ln(m/12)]/2 \tag{32c}$$

$$\beta_4 = [\ln(m/12) + \ln(m/72)]/2 \tag{32d}$$

$$\beta_5 = \beta_6 = 1 \tag{32e}$$

$$\beta_7 = \left(\frac{t_R}{2} - \beta_1\Delta t_1 - \beta_2\Delta t_2 - \beta_3\Delta t_3 - \beta_4\Delta t_4 - 2\tau_D\right)\Big/(\Delta t_7) \tag{32f}$$

where $m = t_R/2\Delta t$ is the total number of spikes and Δt_i gives the duration of the clustered spikes. The values $\Delta t_1 = \Delta t_2 = \Delta t$, $\Delta t_3 = 10\Delta t$, $\Delta t_4 = 60\Delta t$, $\Delta t_5 = \Delta t_6 = \tau_D$ and $\Delta t_7 = t_R/2 - \Sigma_{i=1}^{6}\Delta t_i$ were used, τ_D is the recovery time of the saturable absorber ($\Delta t = 6$ ps used in calculations, $m = 833$).

Equations 13 and 15 for the development of the upper laser level population and intensity in the mode-locking region are rewritten to iterative formulas. The light path along the dash-dotted line of Fig. 1 is followed. The equations for the passage from a to b read ($k = 1$ to K):

$$\begin{aligned} N_{1,ab}(\nu, j, k) = {} & N_{1,cd}(\nu, j-1, k) - \frac{t_R}{2\tau_{sp}} N_{1,cd}(\nu, j-1, k) + J(\nu, j-1)\frac{t_R}{2} \\ & - N_{1,cd}(\nu, j-1, k)\frac{1}{h\nu}\sum_i \int I_{i,ab}(\bar{\nu}, j, k-1)\sigma_{em}(\nu - \bar{\nu})\,d\bar{\nu} \\ & - \frac{N_{1,cd}(\nu, j-1, k) - N_{1,cd}(j-1, k)g_{IH}(\nu - \nu_0)}{T_3}\frac{t_R}{2} \end{aligned} \tag{33}$$

$$\begin{aligned} I_{i,ab}(\nu, j, k) = {} & \left\{ I_{i,ab}(\nu, j, k-1)\exp\left[\Delta z \int N_{1,ab}(\bar{\nu}, j, k)\sigma_{em}(\nu - \bar{\nu})\,d\bar{\nu}\right] \right. \\ & \left. + \frac{h\nu\eta}{\tau_{sp}}\frac{r_A^2}{L_R^2}\Delta t_i N_{1,ab}(\nu, j, k)\Delta z \right\} \frac{1}{1 + \alpha^{(2)}\Delta z I_{i,ab}(j, k-1)/2} \end{aligned} \tag{34}$$

$$I_{i,ab}(j, k-1) = \frac{1}{\Delta t_i}\int I_{i,ab}(\nu, j, k-1)\,d\nu \tag{35}$$

with

$$N_{1,cd}(j-1, k) = \int N_{1,cd}(\nu, j-1, k)\,d\nu \tag{36}$$

From position b to c the light intensity changes to

$$I_{i,cd}(\nu, j, K+1) = I_{i,ab}(\nu, j, K)R_2 T_1^{1/2} \tag{37}$$

The equations for the passage from c to d are similar to Equations 33 to 37. They read ($k = K$ to 1)

$$\begin{aligned} N_{1,cd}(\nu, j, k) = {} & N_{1,ab}(\nu, j, k) - \frac{t_R}{2\tau_{sp}} N_{1,ab}(\nu, j, k) + J(\nu, j-1)\frac{t_R}{2} \\ & - N_{1,ab}(\nu, j, k)\frac{1}{h\nu}\sum_i \int I_{i,cd}(\bar{\nu}, j, k+1)\sigma_{em}(\nu - \bar{\nu})\,d\bar{\nu} \\ & - \frac{N_{1,ab}(\nu, j, k) - N_{1,ab}(j, k)g_{IH}(\nu - \nu_0)}{T_3}\frac{t_R}{2} \end{aligned} \tag{38}$$

$$\begin{aligned} I_{i,cd}(\nu, j, k) = {} & \left\{ I_{i,cd}(\nu, j, k+1)\exp\left[\Delta z \int N_{1,cd}(\bar{\nu}, j, k)\sigma_{em}(\nu - \bar{\nu})\,d\bar{\nu}\right] \right. \\ & \left. + \frac{h\nu\eta}{\tau_{sp}}\frac{r_A^2}{L_R^2}\Delta t_i N_{1,cd}(\nu, j, k)\Delta z \right\} \frac{1}{1 + \frac{1}{2}\alpha^{(2)}\Delta z I_{i,cd}(j, k+1)} \end{aligned} \tag{39}$$

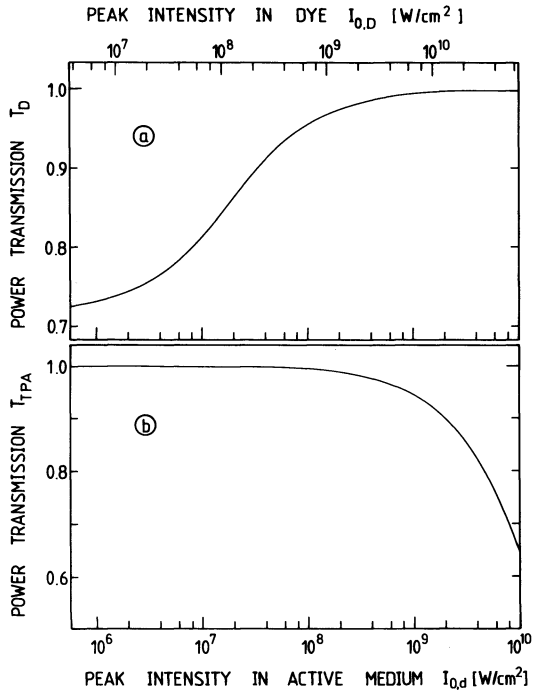

Figure 10 (a) Double-pass light transmission $T_D = \int I_{out}(t)\,dt / \int I_{in}(t)\,dt$ through saturable absorber No. 9860. (b) Double-pass transmission through active medium due to two-photon absorption ($\alpha^{(2)} = 4 \times 10^{-12}\,cm\,W^{-1}$).

$$I_{i,cd}(j, k+1) = \frac{1}{\Delta t_i} \int I_{i,cd}(\nu, j, k+1)\,d\nu \tag{40}$$

with

$$N_{1,ab}(j, k) = \int N_{1,ab}(\nu, j, k)\,d\nu \tag{41}$$

Finally for the passage of light from d through the contacted dye cell back to position a the pulse intensities change to

$$I_{i,ab}(\nu, j+1, 0) = I_{i,cd}(\nu, j, 1) R_1 T_1^{1/2} T_D \tag{42}$$

Equations 33 and 38 describe the population of the upper laser level. The first term gives the initial population. The second term takes care of spontaneous emission while the third term represents the level filling by pumping. The fourth part is responsible for depopulation by stimulated emission. The last contribution includes spectral redistribution due to spectral cross-relaxation. The spectrally integrated level populations $N_{1,ab}(j, k)$ and $N_{1,cd}(j, k)$ are given by Equations 36 and 41, respectively.

Equations 34 and 39 handle the amplification of pulse intensities in the active medium. The first term in the curly brackets is due to amplification of input light. The second term is the contribution from spontaneous emission. The denominator outside the curly brackets is responsible for two-photon absorption [49]. $T_{TPA}(I)$ is depicted in Fig. 10b. The temporal peak intensity of the light pulses is calculated from the spectral intensities by use of Equations 35 and 40 (peak intensity is equal to the intensity of a temporal rectangular pulse of duration Δt).

The nonlinear loss of laser light by passage through the saturable absorber appears in Equation 42. T_D depends on the small signal transmission T_0, the absorption cross-section σ_D and the absorption recovery time τ_D for the dye as well as the input peak intensity and duration of the pulse. The peak intensity of the laser pulses in the dye sample and the active medium differ by a factor f due to different beam focusing and pulse overlap. It is

$$I_{i,D}(j) = f I_{i,cd}(j, 1) \tag{43}$$

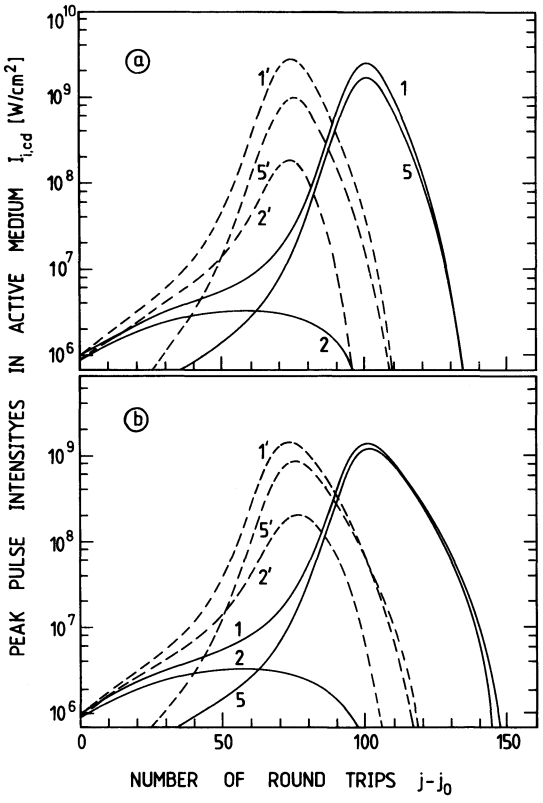

Figure 11 Peak pulse intensities in active medium. (a) Without two-photon absorption. (b) With two-photon absorption $\alpha^{(2)} = 4 \times 10^{-12}\,\mathrm{cm\,W^{-1}}$. Output mirror reflectivity $R_2 = 0.3$. Pump rate $J_0 = 10^{22}\,\mathrm{cm^{-3}\,s^{-1}}$, $j_0 = 74\,800$. Solid curves: initial upper laser level population $N_1(j_0) = 2.0353 \times 10^{18}\,\mathrm{cm^{-3}}$. Dashed curves: $N_1(j_0) = 2.0532 \times 10^{18}\,\mathrm{cm^{-3}}$. 1,1′: most intense pulse $I_{1,cd}(k = 1)$; 2,2′: second most intense pulse $I_{2,cd}(k = 1)$; 5,5′: pulse $I_{5,cd}(k = 1)$ immediately following most intense pulse.

($f \simeq 6.5$ in our experiments, see discussion in Section 4). T_D may be calculated numerically from realistic multilevel systems for the absorber [42, 50]. In the next section we present a simple transient dye model that describes well the nonlinear dye transmission. In the calculations of this section $T_D(I, \Delta t = 6\,\mathrm{ps})$ obtained from the next section is used. It is depicted in Fig. 10a. For the pulses 5 and 6 which immediately follow the most intense pulses 1 and 2 the intensities $I_1 + I_5$ and $I_1 + I_6$ are used for the calculation of T_D since dye transmission increases when a pulse follows within the recovery time of the absorber.

Results of the numerical calculations are displayed in Figs. 11 to 16. The peak pulse intensity versus number of round-trips in the nonlinear laser region are shown in Fig. 11 for a mirror reflectivity of $R_2 = 0.3$ (for the other parameters see Table I). In Fig. 11a two-photon absorption is neglected while in Fig. 11b a two-photon absorption coefficient of $\alpha^{(2)} = 4 \times 10^{-12}\,\mathrm{cm\,W^{-1}}$ is assumed. Two-photon absorption reduces the peak pulse intensity at the pulse train maximum. The solid curves are calculated for a laser level population of $N(j_0) = 2.0353 \times 10^{18}\,\mathrm{cm^{-3}}$, the dashed curves belong to $N_1(j_0) = 2.0523 \times 10^{18}\,\mathrm{cm^{-3}}$ ($J_0 = 1 \times 10^{22}\,\mathrm{cm^{-3}\,s^{-1}}$). At a higher population the pulse train maximum is reached earlier. The development of the most intense pulse (Curves 1 and 1′) the second most intense pulse (Curves 2 and 2′), and the pulse immediately following the most intense pulse (Curves 5 and 5′) are depicted. The pulse discrimination (I_2/I_1) depends critically on the excess pump rate above pump rate threshold. The pulse immediately following the most intense pulse builds up strongly because of reduced saturable dye absorption. In the case of two-photon absorption it increases beyond the preceding pulse towards the end of the pulse train.

Fig. 12a depicts the peak pulse intensity in the laser rod at pulse train maximum versus mirror reflectivity. The higher lying Curves 1 and 2 belong to $\alpha^{(2)} = 0$ while the lower lying Curves 3 and 4 belong to $\alpha^{(2)} = 4 \times 10^{-12}\,\mathrm{cm\,W^{-1}}$. The Curves 1, 3 (solid) and 2, 4 (broken) differ by the minimum amplification ratio $G_1 = I_{10}(j)/I_{10}(j-1)$ in the rising part of the pulse train. With

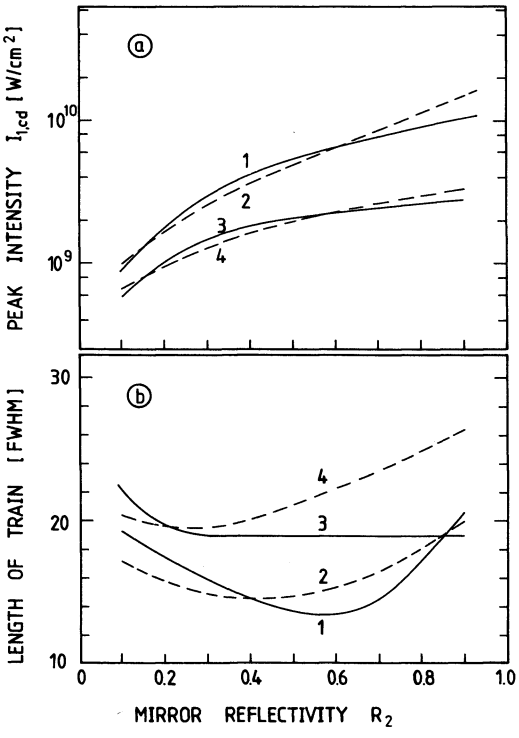

Figure 12 Peak pulse intensity in active medium at pulse train maximum (a) and FWHM-length of pulse train (b) versus mirror reflectivity R_2. Curves: 1, without two-photon absorption $\alpha^{(2)} = 0$ and minimum amplification ratio $G_1 = I_1(j)/I_1(j-1) = 1.02$; 2, $\alpha^{(2)} = 0$ and $G_1 = 1.06$; 3, $\alpha^{(2)} = 4 \times 10^{-12}\,\mathrm{cm\,W^{-1}}$ and $G_1 = 1.02$; 4, $\alpha^{(2)} = 4 \times 10^{-12}\,\mathrm{cm\,W^{-1}}$ and $G_1 = 1.06$.

increasing mirror reflectivity the peak pulse intensity increases. The two-photon absorption levels off the rise of peak pulse intensity with mirror reflectivity.

The dependence of the pulse train length (FWHM) on the mirror reflectivity is plotted in Fig. 12b. The two-photon absorption elongates the pulse trains. The pulse length has a minimum for a reflectivity around 50%.

For the pulse train maximum the intensity ratio of the second most intense pulse I_2 to the most intense pulse I_1 versus minimum amplification ratio in the rising part of the pulse train is shown in Fig. 13 ($\alpha^{(2)} = 0$ in Fig. 13a, $\alpha^{(2)} = 4 \times 10^{-12}\,\mathrm{cm\,W^{-1}}$ in Fig. 13b). The intensity ratio rises strongly with net gain and approaches the value $I_{20}/I_{10} \to 1$. At a fixed minimum amplification ratio the background suppression decreases with increasing mirror reflectivity and increasing two-photon absorption.

The development of the spectral distribution of the upper laser level, of the net gain and of the intensity along the pulse train is depicted in Figs. 14a, b and c, respectively. The figures belong to $R_2 = 0.3$, $N_1(j_0) = 2.0353 \times 10^{18}\,\mathrm{cm^{-3}}$, $J_0 = 1 \times 10^{22}\,\mathrm{cm^{-3}s^{-1}}$ and $\alpha^{(2)} = 4 \times 10^{-12}\,\mathrm{cm\,W^{-1}}$. Towards the pulse train maximum the central region of the upper laser level population $N_1(v)$ is depleted while the wings remain unchanged (spectral hole burning). The net gain for the most intense pulse $G_{net}(v_0)$ (Fig. 14b) slightly reduces in the early part of the nonlinear region (depletion of inversion), then increases to a maximum value (pulse bleaches dye) and decreases below laser threshold ($G_{net}(v_0) < 1$) at the pulse train maximum. Net amplification $G_{net}(v) > 1$ occurs for a longer period at the spectral wings of the pulse.

The total spectral intensity $I(v, j)$ of all pulses within a round trip time is displayed in Fig. 14c. The initial intensity $I(v_0, j - j_0 = 1)$ is rather high compared to the pulse train maximum $I(v_0, j - j_0 = 102)$ because all pulses contribute at the beginning of the nonliner region. In the rising part of the pulse train a minimum in the spectral distribution occurs due to background supression. Towards the end of the pulse train the spectral wings decay more slowly than the central spectrum as a cause of the spectral hole in the upper-laser level population.

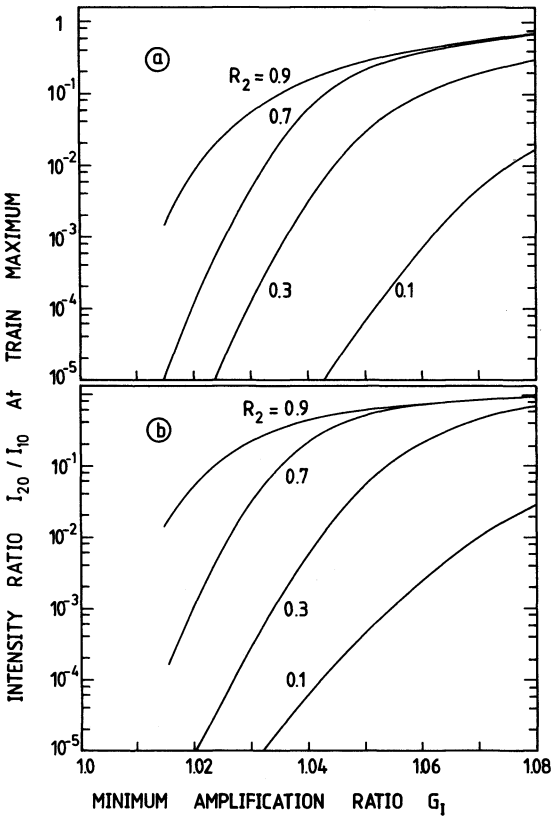

Figure 13 Intensity ratio of second most to most intense pulse at pulse train maximum versus gain for various output mirror reflectivities. (a) Without two-photon absorption $\alpha^{(2)} = 0$; (b) $\alpha^{(2)} = 4 \times 10^{-12}\,\mathrm{cm\,W^{-1}}$.

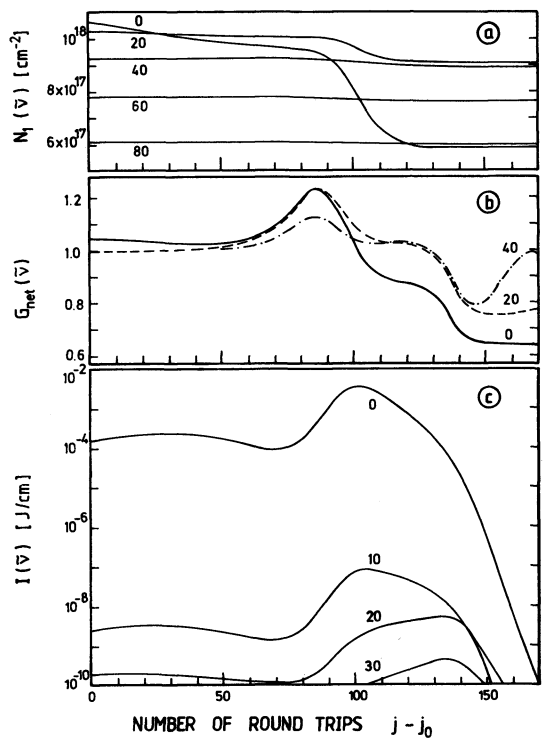

Figure 14 Development of upper laser level population (a), of net gain of most intense pulse (b) and of spectral intensity (c) along pulse train. Numbers at curves indicate frequency positions $\tilde{\nu} - \tilde{\nu}_0$ in $\mathrm{cm^{-1}}$. $R_2 = 0.3$; $N_1(j_0) = 2.0353 \times 10^{18}\,\mathrm{cm^{-3}}$, $\alpha^{(2)} = 4 \times 10^{-12}\,\mathrm{cm\,W^{-1}}$ (see solid curves of Fig. 11b).

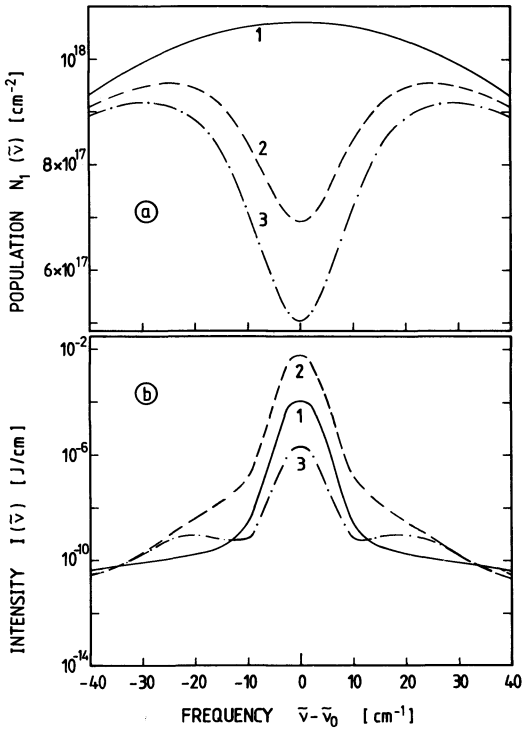

Figure 15 Spectral shape of upper laser level population (a) and of intensity distribution (b) at three different pulse positions. 1, $j - j_0 = 1$ (beginning of nonlinear region); 2, $j - j_0 = 102$ (pulse train maximum); 3, $j - j_0 = 135$ (end of pulse train). Curves belong to $R_2 = 0.3$, $N_1(j - j_0 = 0) = 2.0353 \times 10^{18}\,\mathrm{cm}^{-3}$, $\alpha^{(2)} = 0$ (see solid curves in Fig. 11a).

Fig. 15 shows the spectral hole burning for the situation of $\alpha^{(2)} = 0$, $R_2 = 0.3$, $N_1(j_0) = 2.0353 \times 10^{18}\,\mathrm{cm}^{-3}$ and $J_0 = 1 \times 10^{22}\,\mathrm{cm}^{-3}\,\mathrm{s}^{-1}$ (Fig. 11a, solid curves). In Fig. 15a the upper laser level population versus frequency is depicted for three round trips, one at the beginning of the nonlinear region ($j - j_0 = 1$), one at the pulse train maximum ($j - j_0 = 102$) and one towards the end of the pulse train ($j - j_0 = 135$). The corresponding spectra (integrated over a round trip time) are displayed in Fig. 15b. The build up of spectral peaks in the wings towards the end of the pulse train is seen.

The spectral intensity ratio of the most intense pulse $I_1(20\,\mathrm{cm}^{-1})/I_1(0\,\mathrm{cm}^{-1})$ at the pulse train maximum is shown in Fig. 16b versus mirror reflectivity. It lies between 4×10^{-7} and 2.5×10^{-6}.

6. Temporal pulse development in nonlinear laser region

In the previous section we assumed a constant pulse duration along the pulse train in the nonlinear laser region in resonable agreement with experimental findings. In this section we analyse the temporal pulse development. The problems of spectral changes of the gain profile are not considered. The influence of self-phase modulation is not included.

The laser signal within the transit time t_R is approximated by the most intense spike and an average signal. The temporal intensity distribution $I(t, j_0)$ at the end of the linear phase after j_0 round trips is represented by

$$I(t, j_0) = \bar{I}(j_0)[(2\beta - 1)\exp(-t^2/t_0^2) + 1] \tag{44}$$

$t_0 = \Delta t/2(\ln 2)^{1/2}$ is the 1/e-halfwidth of the fluctuations at the end of the linear phase. Δt is found by $\Delta t \simeq 0.5/\Delta\nu$ where $\Delta\nu$ is the spectral halfwidth at the end of the linear phase (from $\Delta\tilde{\nu} \simeq 1.8\,\mathrm{cm}^{-1}$, see Curve 4 Fig. 8b, follows $\Delta t \simeq 9\,\mathrm{ps}$). $\bar{I}(j_0)$ is the average pulse intensity at the end of the linear phase (Equation 26). β is given by Equation 32a ($m = 556$, $\beta = 6.7$). The factor 2 before β in Equation 44 is due to the fact that the peak pulse is a factor of 2 higher than the average pulse intensity.

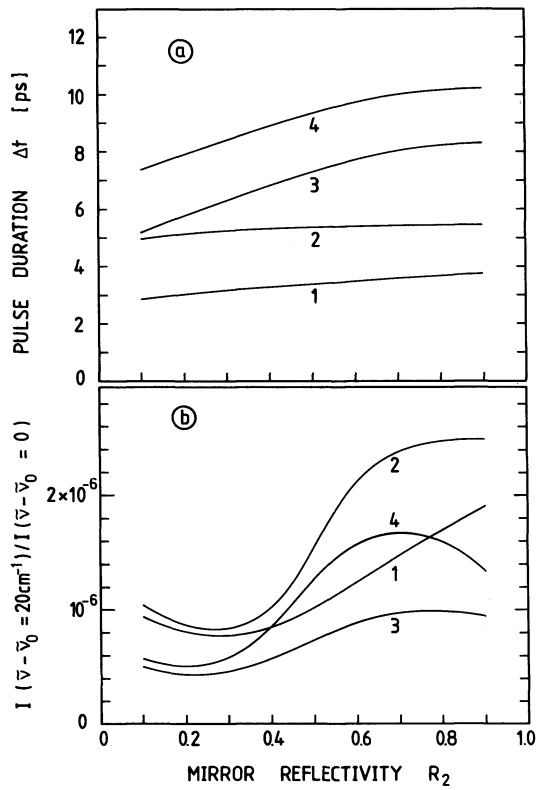

Figure 16 Pulse duration Δt (a) and total spectral intensity ratio $I(\tilde{\nu} - \tilde{\nu}_0 = 20\,\mathrm{cm}^{-1})/I(\tilde{\nu} - \tilde{\nu}_0 = 0)$ versus mirror reflectivity. Curves belong to 1: $\alpha^{(2)} = 0$, $G_1 = 1.02$; 2: $\alpha^{(2)} = 0$, $G_1 = 1.06$; 3: $\alpha^{(2)} = 4 \times 10^{-12}\,\mathrm{cm\,W^{-1}}$, $G_1 = 1.02$; 4: $\alpha^{(2)} = 4 \times 10^{-12}\,\mathrm{cm\,W^{-1}}$, $G_1 = 1.06$.

The interaction of the light pulses with the active medium is approximated by (a) neglecting the population of the lower laser level $N_2 = 0$; (b) the total upper laser level population is assumed to interact, i.e. $N_1(j_0) = \int N_1(\nu, j_0)\,\mathrm{d}\nu$. The stimulated emission cross-section is set to $\bar{\sigma}_{\mathrm{em},0}$ (inhomogenous effects are not explicitly discussed).

Equations 33 to 42 reduce to

$$N_{1,\mathrm{ab}}(j) = N_{1,\mathrm{cd}}(j-1) - \frac{t_R}{2\tau_{sp}} N_{1,\mathrm{cd}}(j-1) + J(j-1)\frac{t_R}{2} - N_{1,\mathrm{cd}}(j-1)\left\{\exp\left[\frac{\bar{\sigma}_{\mathrm{em},0}}{h\nu_0}\int_{-3t_0}^{t_R-3t_0} I_a(t,j)\,\mathrm{d}t\right] - 1\right\} \tag{45}$$

$$I_b(t,j) = \left[\int_{-3t_0}^{t} I_a(t',j)g(t'-t)\,\mathrm{d}t' + \bar{I}_{\mathrm{sp,ab}}(j)\right]\frac{\exp\left[l_a\bar{\sigma}_{\mathrm{em},0}N_{1,\mathrm{ab}}(j)\right]}{1 + \alpha^{(2)}l_R I_a(t,j)} \tag{46}$$

$$I_c(t,j) = I_b(t,j)R_2 T_1^{1/2} \tag{47}$$

$$N_{1,\mathrm{cd}}(j) = N_{1,\mathrm{ab}}(j) - \frac{t_R}{2\tau_{sp}} N_{1,\mathrm{ab}}(j) + J(j-1)\frac{t_R}{2} - N_{1,\mathrm{ab}}(j)\left\{\exp\left[\frac{\bar{\sigma}_{\mathrm{em},0}}{h\nu_0}\int_{-3t_0}^{t_R-3t_0} I_c(t,j)\,\mathrm{d}t\right] - 1\right\} \tag{48}$$

$$I_d(t,j) = \left\{\int_{-3t_0}^{t} I_c(t',j)g(t'-t)\,\mathrm{d}t' + \bar{I}_{\mathrm{sp,cd}}(j)\right\}\frac{\exp\left[l_A\bar{\sigma}_{\mathrm{em},0}N_{1,\mathrm{cd}}(j)\right]}{1 + \alpha^{(2)}l_R I_c(t,j)} \tag{49}$$

$$I_a(t,j+1) = I_d(t,j)R_1 T_1^{1/2} T_D(t,j) \tag{50}$$

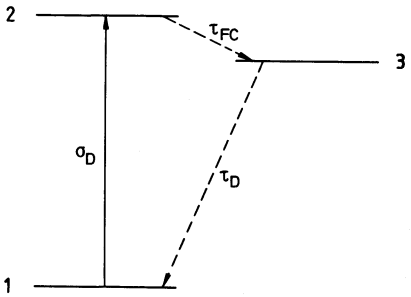

Figure 17 Level diagram for saturable absorber.

$g(t' - t)$ is the response function of the active medium. It takes care of the temporal pulse broadening effect by the finite spectral width of the gain profile (natural mode selection). In the calculations $\int_{-\infty}^{t} I(t', j)g(t' - t)\,dt'$ is approximated by $I(\xi t, j)$ where $\xi = [\Delta t(j)^2 + \Delta t_{IH}^2]^{1/2}/\Delta t(j)$ is the pulse broadening factor. $\Delta t_{IH} \simeq 0.5/\Delta\nu_{IH} \approx 8 \times 10^{-14}$ s is the characteristic response time of the active medium.

The transmission $T_D(t, j)$ of a light pulse through a saturable absorber is generally obtained by solving a coupled differential equation system for the level populations of the dye and the intensity changes along the sample [42, 46, 50]. Here we use a heuristic model of transient dye bleaching that allows an easy calculation of pulse shape changes and transmission [43, 44]. The dye molecules are described by a three-level system with a fast intermediate state (see Fig. 17; $\tau_{FC} \to 0$). Excited state absorption of Kodak No. 9860 is weak ($\sigma_{ex} = 2.5 \times 10^{-17}$ cm^2 [55]) and is neglected here. The transmission of a pulse at time position $t' = t - cz/n$ moving with propagation velocity c/n is

$$T_D(t', j) = T_0 \exp\left[\kappa\sigma_D N_{D,3}(t', j)\right] \tag{51}$$

T_0 is the double-pass small signal dye transmission through the contacted dye cell. $N_{D,3}(t', j)$ is the total number of excited dye molecules at time t' (integrated over double path length of sample; dimension: cm^{-2}). σ_D denotes the isotropic absorption cross-section. The correction factor κ takes care of the absorption anisotropy of electric dipole interaction in an approximate manner ($\kappa = 2$ is used in calculations).

The total number of excited molecules $N_{D,3}$ is obtained by counting the number of absorbed laser photons accounting for the relaxation of excited molecules:

$$N_{D,3}(t', j) = \int_{-3t_0}^{t'} \frac{I_D(\tilde{t}, j)}{h\nu_0}\left[1 - T_D(\tilde{t}, j)\right] \exp\left[-(t' - \tilde{t})/\tau_D\right] d\tilde{t} \tag{52}$$

$(-3t_0 < t' < t_R - 3t_0)$. The pulse intensity in the contacted dye cell $I_D(t', j)$ is related to the pulse intensity $I_d(t', j)$ in the active medium at position d (Fig. 1) by $I_D(t', j) = fI_d(t', j)$ (see Equation 43).

The pulse intensities I_d in the active medium versus the number of round trips in the nonlinear phase are shown in Figs. 18a and 19a for $\alpha^{(2)} = 0$ and $\alpha^{(2)} = 4 \times 10^{-12}$ cm W^{-1}, respectively. The mirror reflectivity is $R_2 = 0.3$ and the pump rate is $J_0 = 1 \times 10^{22}$ cm^{-3}s^{-1}. The small signal double-pass dye transmission is $T_0 = 0.7225$ (for other parameters see Table I). The solid and broken curves belong to upper laser level population of $N_1(j_0 = 0) = 2.059 \times 10^{18}$ cm^{-3} and 2.009×10^{18} cm^{-3}, respectively. As in Section 4 the two-photon absorption lowers the peak pulse intensity at the pulse train maximum and increases the length of the pulse train. The peak intensities at the pulse train maximum are higher than in Fig. 11 since only qne pulse with background is considered here.

In Figs. 18b and 19b the corresponding pulse durations along the pulse train are depicted. Without two-photon absorption the pulse durations shorten in the early rising part of the pulse train. Then the pulse duration remains constant around the pulse train maximum since the dye is

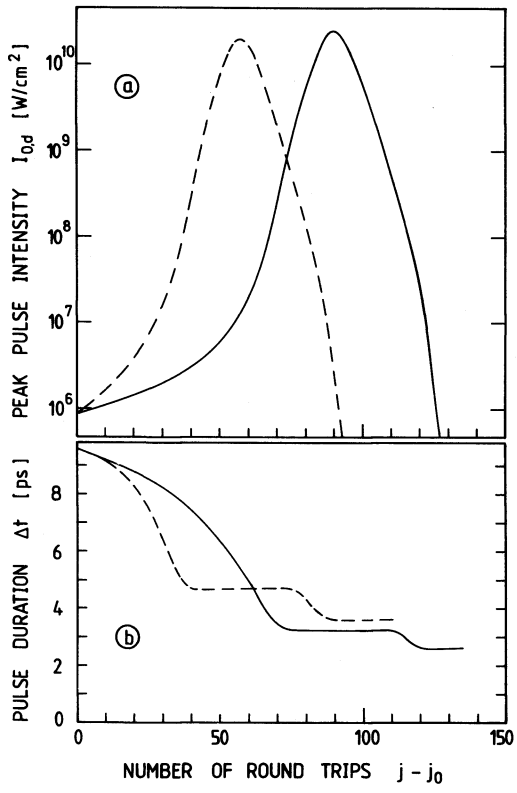

Figure 18 Development of peak intensity in active medium (a) and pulse duration (b) along pulse train. Solid curves: $N_1(j_0) = 2.009 \times 10^{18}\,\mathrm{cm}^{-3}$; dashed curves: $N_1(j_0) = 2.0532 \times 10^{18}\,\mathrm{cm}^{-3}$. Without two-photon absorption, $R_2 = 0.3$, pump rate $J_0 = 1 \times 10^{22}\,\mathrm{cm}^{-3}\mathrm{s}^{-1}$.

completely bleached. In the trailing part of the pulse train a further region of pulse shortening is passed when the pulse intensity enters the region of partial dye bleaching. In case of two-photon absorption (Fig. 19b) the pulse durations increase around the pulse train maximum since the peaks of the pulses are preferentially absorbed.

In Fig. 20 the temporal pulse shapes for some pulse train positions are shown. Part (a) belongs to $\alpha^{(2)} = 0$, part (b) to $\alpha^{(2)} = 4 \times 10^{-12}\,\mathrm{cm\,W}^{-1}$. The parameters are identical to the solid curves in Figs. 18 and 19 [$N_1(j_0) = 2.009 \times 10^{18}\,\mathrm{cm}^{-3}$]. The steep rise and the maximum shift of the pulses due to pronounced absorption in the rising part of the pulse shape are clearly seen. The two-photon absorption cuts the peaks of the pulses.

In Fig. 16a the dependence of the pulse duration at the pulse train maximum on the mirror reflectivity is depicted for two cases of minimum amplification ratio in the rising part of the pulse train and two cases of two-photon absorption. The pulse durations increase slightly with mirror reflectivity. Higher initial net gain results in longer pulse durations. The two-photon absorption broadens the pulse duration.

7. Effects of self-phase modulation

Self-phase modulation broadens and modulates the pulse spectra along the pulse train [10, 20, 23, 25, 56–63]. The effect accumulates with the number of round trips. Self-phase modulation in dispersive media influences the temporal pulse development and may lead to temporal pulse substructure [25, 56, 57, 64–70]. Negative dispersion leads to pulse envelope compression; positive dispersion results in pulse envelope broadening. Pulse compression of self-phase modulated pulses in grating pairs is a frequently used technique of pulse shortening [64, 71–75]. Here we study the influence of the spectral gain profile on the spectral and temporal pulse development.

The self-phase modulation is caused by the intensity dependence of the refractive index n at high

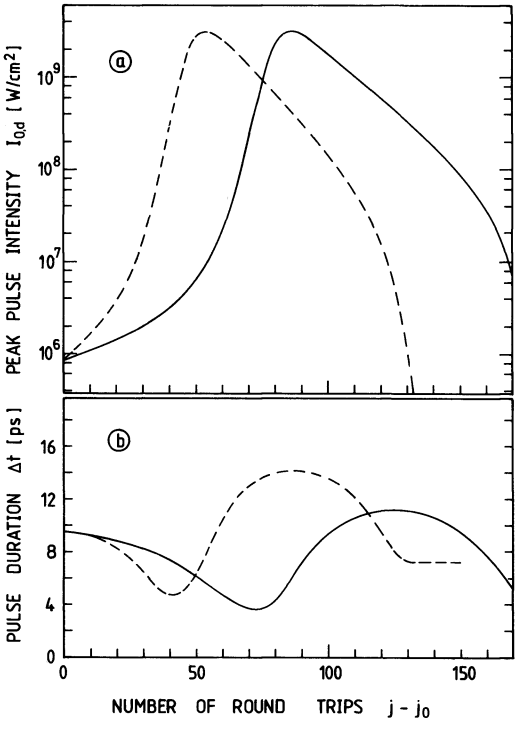

Figure 19 Peak intensity $I_{0,d}$ in active medium (a) and pulse duration (b) along pulse train. Solid curves: $N_1(j_0) = 2.009 \times 20^{18}\,\mathrm{cm}^{-3}$; dashed curves: $N_1(j_0) = 2.0532 \times 10^{18}\,\mathrm{cm}^{-3}$, $\alpha^{(2)} = 4 \times 10^{-12}\,\mathrm{cm\,W}^{-1}$, $R_2 = 0.3$, $J_0 = 1 \times 10^{22}\,\mathrm{cm}^{-3}\,\mathrm{s}^{-1}$.

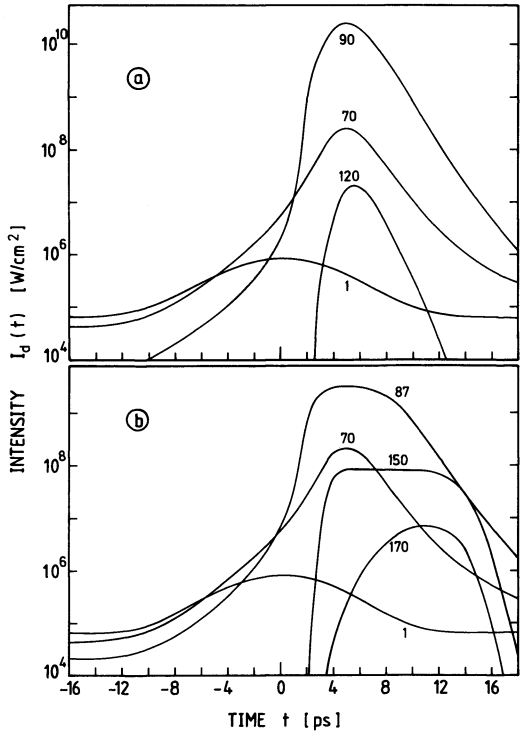

Figure 20 Temporal pulse shape at various positions along pulse train. (a) Parameters are equal to the solid curves of Fig. 18 ($\alpha^{(2)} = 0$, $N_1(j_0) = 2.009 \times 10^{18}\,\mathrm{cm}^{-3}$). (b) Parameters are the same as for the solid curves of Fig. 19 ($\alpha^{(2)} = 4 \times 10^{-12}\,\mathrm{cm\,W}^{-1}$, $N_1(j_0) = 2.009 \times 10^{18}\,\mathrm{cm}^{-3}$). Numbers on the curves indicate round trip positions $j - j_0$.

laser intensities [21–26]. The time dependent refractive index is (assuming instant response):

$$n(t) = n_0 + \frac{n_2}{2}|E_0(t)|^2 = n_0 + \gamma I(t) \tag{53}$$

n_0 is the refractive index at low intensities. n_2 or $\gamma = n_2/(n_0 c\varepsilon_0)$ describe the intensity dependence of the refractive index.

The wave propagation of an electrical field is given by

$$E(t, z) = E_0(t, z) \exp[\mathrm{i}(\omega_0 t - kz)] \tag{54}$$

E_0 is the electrical field amplitude and k is the wave vector. The latter is given by

$$k = n\frac{\omega_0}{c} = n_0\frac{\omega_0}{c} + \gamma I\frac{\omega_0}{c} \tag{55}$$

Using the transformation $t' = t - n_0 z/c$ Equation 54 reads

$$E(t', z) = \tilde{E}_0(t', z) \exp(\mathrm{i}\omega_0 t') \tag{56}$$

with

$$\begin{aligned}\tilde{E}_0(t', z) &= E_0(t', z) \exp\left[-\mathrm{i}\frac{\omega_0}{c}\gamma I(t')z\right] \\ &= |E_0(t', z)| \exp[-\mathrm{i}\phi(t', z)]\end{aligned} \tag{57}$$

where

$$E_0(t', z) = |E_0(t', z)| \exp(-\mathrm{i}\varphi) \quad \text{and} \quad \phi(t', z) = \frac{\omega_0}{c}\gamma I(t')z + \varphi$$

The spectral field strength is found by Fourier transforming Equation 56:

$$E(\omega, z) = F[E(t', z)] = \int_{-\infty}^{\infty} \tilde{E}_0(t', z) \exp[-\mathrm{i}(\omega - \omega_0)t']\,\mathrm{d}t' \tag{58}$$

The transformation $\omega' = \omega - \omega_0$ leads to

$$E(\omega', z) = \int_{-\infty}^{\infty} \tilde{E}_0(t', z) \exp(-\mathrm{i}\omega' t')\,\mathrm{d}t' = F[\tilde{E}_0(t', z)] \tag{59}$$

Finally the spectral intensity distribution is given by

$$I(\omega', z) = \frac{cn_0\varepsilon_0}{4\pi}|E(\omega', z)|^2 \tag{60}$$

The relation between $I(\omega')$ and $I(\tilde{\nu}')$ ($\tilde{\nu}'$ in cm^{-1}) is given by the energy conservation

$$\int_{-\infty}^{\infty} I(\omega')\,\mathrm{d}\omega' = \int_{-\infty}^{\infty} I(\tilde{\nu}')\,\mathrm{d}\tilde{\nu}' = 2\pi c\int_{-\infty}^{\infty} I(\omega')\,\mathrm{d}\tilde{\nu}' \quad \text{i.e. } I(\tilde{\nu}') = 2\pi c I(\omega').$$

A complete calculation of the temporal and spectral pulse development in the oscillator including all circulating pulses and the spontaneous emission is very time consuming. We therefore use a simple model of only one pulse within the cavity. A sine-shaped pulse train is assumed with peak pulse intensities

$$I_0(j) = I_{0,\max}\sin(\pi j/M) \tag{61}$$

(see Fig. 21a) and with an initial temporal shape of

$$\begin{aligned}I(t', j = 1, z = 0) = I_0(j = 1)\{&\exp(-t'^2/t_0^2)[1 - \theta(t' - \Delta t_1)] \\ &+ \exp(-\Delta t_1^2/t_0^2)\cosh(\Delta t_1/\kappa_t t_0)\theta(t' - \Delta t_1)/\cosh(t'/\kappa_t t_0)\}\end{aligned} \tag{62}$$

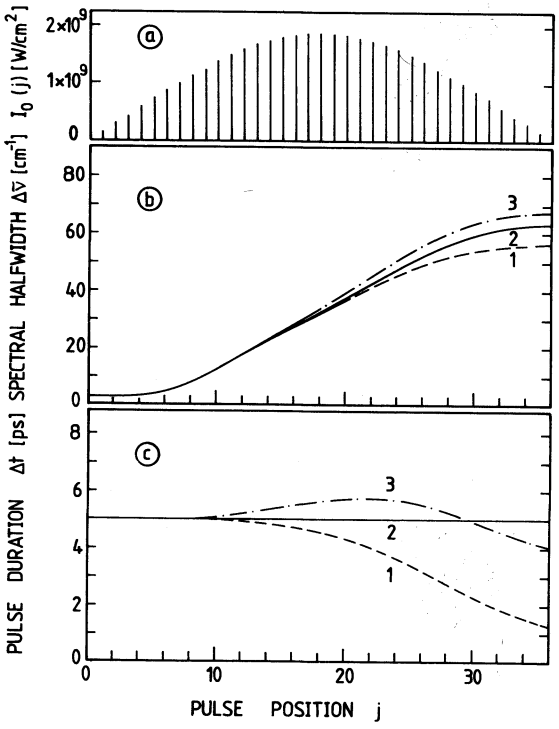

Figure 21 Influence of self-phase modulation on spectral halfwidth (b) and pulse duration (c) for pulse train (a). Initial pulse shape: asymmetric (see solid curve in Fig. 24). Initial duration: 5 ps. Nonlinear constant $\gamma = 3 \times 10^{-16}\,\mathrm{cm^2 W^{-1}}$. Curves: 1 (dashed), gaussian gain profile ($\tilde{\nu}_G = 113\,\mathrm{cm^{-1}}$); 2 (solid), constant gain; 3 (dash-dotted) gain simulates spectral hole. Gain distributions are shown in Fig. 22.

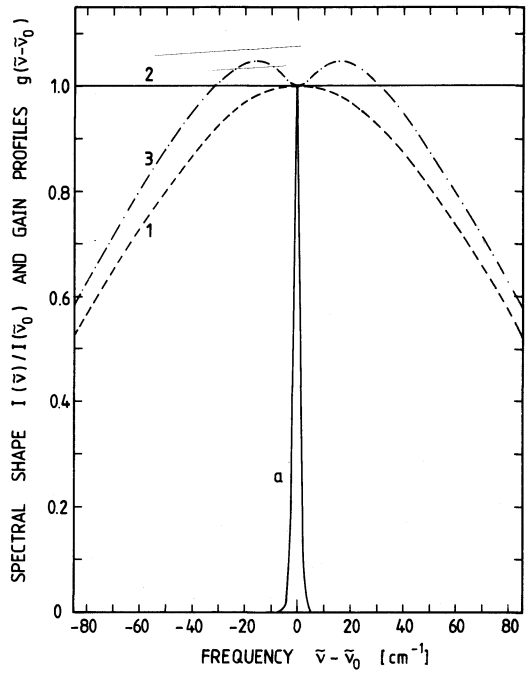

Figure 22 Spectral gain distributions (1–3) and initial spectral pulse shape (a).

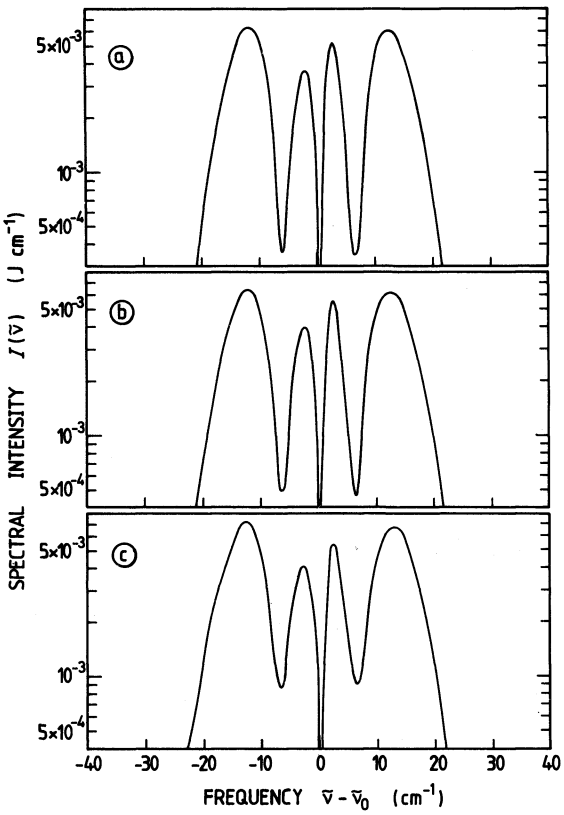

Figure 23 Spectral shapes due to self-phase modulation at pulse train maximum of Fig. 21a ($j = 18$). (a) gaussian gain, (b) constant gain, (c) inhomogeneous gain with spectral hole (see Fig. 22). $\gamma = 3 \times 10^{-16}\,\mathrm{cm^2\,W^{-1}}$.

(see solid curves in Figs. 24 and 26. The corresponding Fourier transformed spectral shape is shown by Curve a in Fig. 22). The initial electrical field distribution is

$$|\tilde{E}_0(t', j = 1, z = 0)| = \left[\frac{2}{n_0 c \varepsilon_0} I(t', j = 1, z = 0)\right]^{1/2} \tag{63}$$

and

$$\phi(j = 1, z = 0) = \varphi_1 \tag{64}$$

In the calculations we use $I_{0,\max} = 2 \times 10^9\,\mathrm{W\,cm^{-2}}$, $M = 36$, $\Delta t_1 = 2[\ln 2]^{1/2} t_0 = 5\,\mathrm{ps}$, $\kappa_t = 1.6$ (asymmetric pulse shape) and $\varphi_1 = 0$. $\theta(t) = 0$ for $t < 0$ and $\theta(t) = 1$ for $t > 0$ is a step function.

The temporal and spectral pulse development along the pulse train is calculated by the following iteration

$$E(\omega', j, z = 0) = F[\tilde{E}_0(t', j, z = 0)] \tag{65}$$

$$E(\omega', j, z = 2l_R) = [g(\omega')]^{1/2} E(\omega', j, z = 0) \tag{66}$$

$$\begin{aligned}\tilde{E}_0(t', j, z = 2l_R) &= F^{-1}[E(\omega', j, z = 2l_R)] \\ &= |\tilde{E}_0(t', j, z = 2l_R)| \exp[-i\phi(t', j, z = 2l_R)]\end{aligned} \tag{67}$$

$$I(t', j, z = 2l_R) = \frac{n_0 c \varepsilon_0}{2} |\tilde{E}_0(t', j, z = 2l_R)|^2 \tag{68}$$

$$|\tilde{E}_0(t', j + 1, z = 0)| = |\tilde{E}_0(t', j, z = 2l_R)| \left\{\frac{I(t', j, z = 2l_R)}{[I(t'_{\max}, j, z = 2l_R)]}\right\}^{1/2} \tag{69}$$

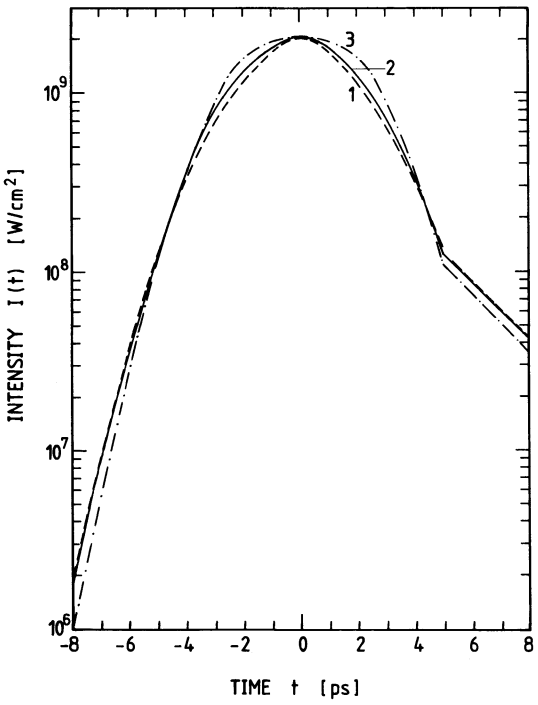

Figure 24 Temporal pulse shapes due to self-phase modulation at pulse train maximum of Fig. 21a (j = 18). Curves: 1, gaussian gain; 2, constant gain (shape unaffected);3, inhomogeneous gain with spectral hole (same parameters as in Fig. 23).

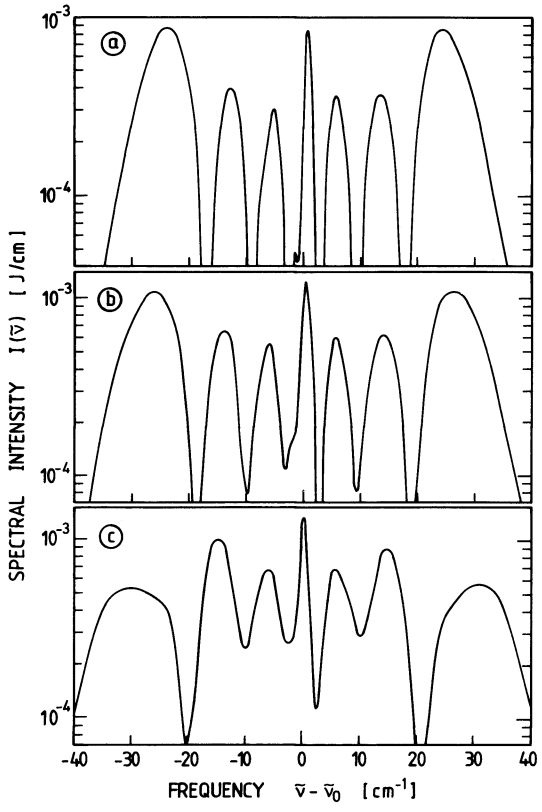

Figure 25 Spectral intensity distributions due to self-phase modulation towards end of pulse train of Fig. 21a (j = 33). (a) gaussian gain, (b) constant gain, (c) gaussian gain with spectral hole (see Fig. 22).

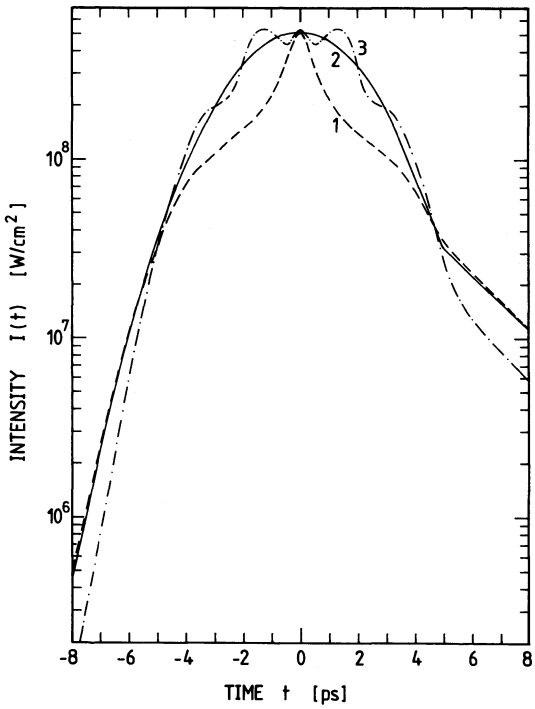

Figure 26 Temporal pulse shapes corresponding to Fig. 25. 1, gaussian gain; 2, constant gain; 3, spectral hole in gaussian gain profile.

$$\phi(t', j+1, z=0) = \phi(t', j, z=2l_R) + \varphi(j+1) + \frac{\omega_0}{c}\gamma I(t', j, z=2l_R)2l_R \tag{70}$$

where t'_{max} is the time position where $I(t')$ has its maximum. To study the influence of the spectral gain distribution three gain distributions $g(\nu') = g(\omega'/2\pi)$ are used:

$$g(\nu') = \exp(-\nu'^2/\nu_G^2) \tag{71a}$$

$$g(\nu') = 1 \tag{71b}$$

$$g(\nu') = \left\{1 + h\left[1 - \frac{\Delta\nu_H^2/4}{\nu'^2 + (\Delta\nu_H/2)^2}\right]\right\} \exp(-\nu'^2/\nu_G^2) \tag{71c}$$

These distributions are depicted in Fig. 22. Curve 1 (Equation 71a) simulates a homogeneous gain medium. Curve 2 (Equation 71b) neglects the spectral gain dependence. Curve 3 (Equation 71c) represents the spectral hole burning in an inhomogeneous gain medium ($h = 0.1$ is used).

Fig. 21b shows the spectral halfwidth versus pulse position. For the used spectral gain profiles nearly the same spectral broadening is observed. The dependence of the pulse duration on the pulse position is shown in Fig. 21c. In case of constant spectral gain (Equation 71b) the temporal pulse shape remains unchanged (see solid curves in Figs. 24 and 26) and the pulse duration remains constant. The gaussian gain profile (Equation 71a) leads to a shortening of the pulse duration. The temporal pulse shape at the peak is narrowed (dashed curve in Fig. 24 for $j = 18$, pulse train maximum) and the shoulders build up (dashed curve in Fig. 26 for $j = 33$, end of pulse train). For higher pulse intensities ($I_{0,max}$), longer pulse trains (M), or larger γ-values the shoulders would grow up to side peaks and the total pulse duration (FWHM) of the formed three subpulses would slightly increase above the initial value. The gain profile belonging to a spectral hole (Equation 71c) leads to a slight modulation of the pulse duration around the initial value (dash dotted curves in Figs. 21c, 24 and 26). After initial pulse broadening (Fig. 24, $j = 18$), the pulse breaks up into three subpulses (Fig. 26, $j = 33$). For higher nonlinearities the subpulses break up further.

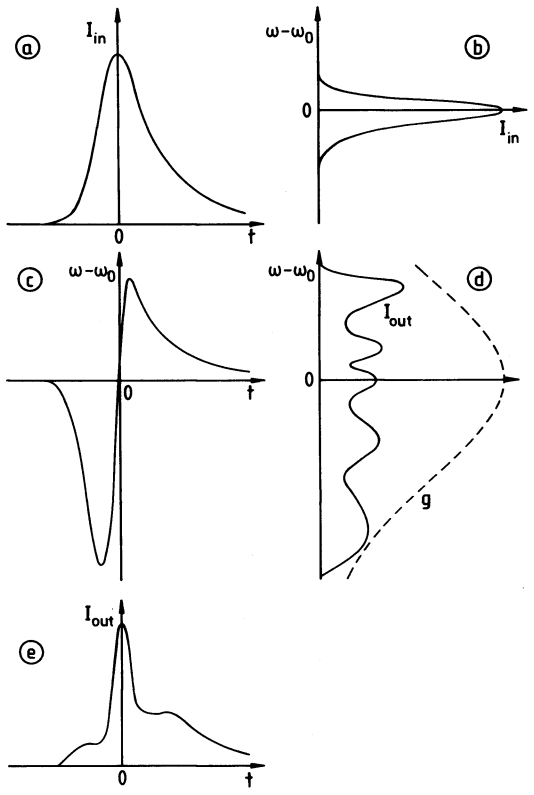

Figure 27 Graphical analysis of spectral–temporal pulse development due to self-phase modulation. (a) Temporal input pulse shape; (b) spectral input pulse shape; (c) wave frequency versus time of picosecond pulse; (d) gain distribution $g(\omega - \omega_0)$ and spectral output pulse shape; (e) temporal output pulse shape.

Spectral distributions at the pulse train maximum ($j = 18$) and the end of the pulse train ($j = 33$) are shown in Figs. 23 and 25, respectively for the three discussed gain profiles. The spectral asymmetry is due to the initial asymmetric temporal pulse shape (Equation 62). The number of modulation spikes increases with $\phi(t')$ (Equation 70). (The spectra are not integrated over the spatial beam profile).

The temporal spectral pulse development due to self-phase modulation may be visualized without the need of Fourier transforms [26, 76]. A graphical analysis is outlined in Fig. 27. An asymmetric input pulse $I_{in}(t)$ is shown in part (a) (steep leading and slow trailing edge). The corresponding spectral input pulse distribution $I_{in}(\omega)$ is depicted in part (b). The self-phase modulation changes the wave frequency ω_0 of an unmodulated pulse to $\omega(t) = \omega_0 - \partial\phi/\partial t = \omega_0 - (\omega_0/c)\gamma\partial I/\partial t$ as illustrated in Fig. 27c. The spectrally broadened pulse is amplified (attenuated) according to the spectral gain distribution $g(\omega - \omega_0)$ (see Fig. 27d). The output spectrum (Fig. 27d) is modulated due to interference effects: along the time axis a fixed wave frequency $\bar{\omega} - \omega_0$ appears at two different times $\bar{t}_1$ and $\bar{t}_2$. If $\Delta\phi = (\bar{\omega} - \omega_0)(\bar{t}_2 - \bar{t}_1) = 2n\pi$ (integer n) the waves interfere constructively. On the other hand, if $\Delta\phi = (2n + 1)\pi$ then destructive interference occurs. The number of spectral interference fringes may be used to determine the input pulse duration [77]. The spectral asymmetry gives information on the temporal asymmetry of the input pulse. Fig. 28e depicts the temporal output pulse shape $I_{out}(t)$. The spectral gain $g(\omega - \omega_0)$ together with the temporal dependence of the wave frequency $\omega(t)$ of the pulse alters the temporal output pulse shape. The bell-shaped distribution $g(\omega - \omega_0)$ of Fig. 27d reduces the spectral wings. The spectral extrema coincide with the temporal inflection points. The reduced gain at the inflection points leads to the depicted temporal pulse modulation (shortening of pulse duration, break up into three subpulses, in further passage each subpulse may break up into three short pulses). A constant gain, $g(\omega - \omega_0) =$ constant, does not change the temporal pulse shape.

The experimental observation of temporal substructure of picosecond pulses was reported in [25, 56, 57, 64–70]. The shortening of mode-locked Nd–Yag laser pulses towards the end of the pulse train [78] may be explained by the mechanism leading to Curve 1 of Fig. 26. A pulse break up into three subpulses towards the end of the pulse train was observed in a mode-locked ruby laser [79]. The effect is thought to be caused by self-phase modulation in a homogeneously broadened gain medium.

In the calculations $\varphi(j) =$ constant was assumed. If $\varphi(j)$ becomes time dependent (towards phase incoherence between round trips) then the calculations presented break down (Fourier and inverse Fourier transforms) and the spectral distribution may be amplified according to the gain profiles. This fact would cause preferential amplification of the wings in case of spectral hole distribution as was found experimentally [19, 20].

8. Other influences on pulse formation

Up to now the influence of self-focusing [67, 68, 80] and optical dispersion [69] has been neglected.

The intensity dependence of the refractive index causes beam focusing due to the spatial intensity distribution of the laser pulse. The self-focusing length for the active medium is [81, 82].

$$z_f = \frac{kw^2}{2}\left(\frac{P}{P_c} - 1\right)^{-1/2} \tag{72}$$

with the wave number $k = 2\pi/\lambda$, the spot size in the active medium $w = w_0(1 + 4z^2/b^2)^{1/2}$, the laser power $P = \pi w^2 I_0$, and the critical power $P_c = c\varepsilon_0\lambda^2/(4\pi n_2)$. $w_0 = (\lambda b/2\pi)^{1/2}$ is the minimum spot size in the laser resonator, b is the curvature of the output mirror (the front mirror is plane in our system). For our experimental data ($\lambda = 1.053\,\mu$m, $z = 90$ cm, $b = 3$ m, $n_2 = 1.2 \times 10^{-22}\,\mathrm{m^2\,V^{-2}}$ [83]) the self-focusing length becomes equal to the rod length $l_R = 13$ cm at $I_0 = 3 \times 10^{10}\,\mathrm{W\,cm^{-2}}$. Due to the two-photon absorption in the active medium the peak intensity in the laser rod is limited to $I_0 \lesssim 2 \times 10^9\,\mathrm{W\,cm^{-2}}$ for our experimental conditions ($T_0 = 0.85^2$ see Fig. 11). The self-focusing process would limit the extractable laser intensity to $I_0 < 3 \times 10^{10}\,\mathrm{W\,cm^{-2}}$. For $I_0 = 2 \times 10^9\,\mathrm{W\,cm^{-2}}$ the self-focusing length is $z_f \simeq 52$ cm. This length is long compared to the rod length. Within the rod the beam is only slightly focused and the beam propagation may be described by a resonator with slightly changed curvature of the mirrors. Under certain experimental conditions (higher saturable absorber concentration, other mirror curvatures, longer rods, lower two-photon absorption cross-sections, small aperture width) the wave front bending by the nonlinear lens effect of the active medium may limit the peak intensity at the maximum of the pulse train and may lead to pulse trains with two or more maxima [67, 80, 84].

The optical dispersion of the refractive index $n = n_0 + (\partial n/\partial\tilde{\nu})\Delta\tilde{\nu}$ leads to a temporal broadening Δt_{disp} of the light pulses per round trip

$$\Delta t_{disp} = \frac{2l_R}{c}\frac{\partial n}{\partial\tilde{\nu}}\Delta\tilde{\nu}$$

For typical values of $\partial n/\partial\tilde{\nu} = 1.4 \times 10^{-6}$ cm [83] and $\Delta\tilde{\nu} = 5\,\mathrm{cm^{-1}}$ one finds $\Delta t_{disp} \approx 6 \times 10^{-15}$ s. This value is negligibly small compared to other shortening (saturable absorber) and broadening (two-photon absorption, finite gain width) effects [43, 44]. The influence of optical dispersion on pulse break-up of self-phase modulated pulse was mentioned in Section 7.

9. Comparison with experiments and conclusions

The experimental spectral pulse development was investigated by Penzkofer and Weinhardt [19, 20] (Curves 5 and 6 of Fig. 7 in [20] could not be reproduced). Towards the end of the pulse train the spectral peak shifted to the wings. In Section 5 the gain depletion at the centre frequency was

analysed. An enlarged amplification of the spectral wings was found but the intensity at the centre frequency dominated. The self-phase modulation (Section 7) modulates and broadened the spectrum. The coherent interaction of the modulated pulse with the gain medium hinders a pronounced growth of the spectral wings. It is thought that for the experiments of Penzkofer and Weinhardt [19, 20] the self-phase modulation broadened the spectra and that the broadened pulses lost part of their coherence so that the wings were amplified according to the high gain acting at the wings.

The experimental temporal pulse development [20, 43, 44] is in agreement with the theoretical predictions of Sections 6 and 7.

The detailed theoretical analysis of temporal and spectral pulse development gives the possibility to improve the mode-locking action. The laser frequency may be fixed to the centre frequency along the whole pulse train using a Fabry–Perot etalon with its transmission maximum at the centre laser frequency. The laser frequency may be tuned within the inhomogeneous gain profile by tilting the etalon.

Several possibilities of temporal pulse shortening exist:

1. With rightly adjusted thin glass plates the natural mode selection may be partially compressed and shorter pulses generated ([43] and references therein).

2. The resonator losses may be increased in the rising part of the pulse train with a Pockels cell-polarizer system in order to keep the pulse intensity in the region of optimum pulse shortening by the saturable absorber [44].

3. Two saturable absorbers with different saturation intensity and different absorption recovery time may be inserted in the oscillator [46, 79]. The dye with the lower saturation intensity starts the mode-locking action. The dye with the higher saturation intensity and shorter relaxation time extends the region of pulse shortening.

4. The mode-locking action may be started in a master oscillator with low saturable absorber concentration and in the rising part of the pulse train the circulating pulse may be switched over to a slave oscillator with high saturable absorber concentration and its own active medium [85].

5. A switchover to a side arm of the original oscillator which contains a saturable dye cell with high concentration may be used. This arrangement needs only one active medium [84, 86]. Pulse durations down to 0.4 ps have been generated in such a mode-locked laser oscillator [84].

6. Saturable dyes with shorter absorption recovery time allow the generation of shorter pulses [13, 48]. The application of a dye with subpicosecond recovery time has led to subpicosecond pulse generation in a laser oscillator [87].

References

1. V. S. LETOKHOV, *Sov. Phys. JETP* **28** (1969) 562.
2. J. A. FLECK, *Phys. Rev.* **A1** (1970) 84.
3. R. M. PICARD and P. SCHWEITZER, *ibid.* **A1** (1970) 1803.
4. P. G. KRYUKOV and V. S. LETOKHOV, *IEEE J. Quant. Electron.* **QE-8** (1972) 766.
5. B. Ya. ZEL'DOVICH and T. T. KUZNETSOVA, *Sov. Phys. USPEKI* **15** (1972) 25.
6. W. H. GLENN, *IEEE J. Quant. Electron.* **11** (1975) 8.
7. R. WILBRANDT and H. WEBER, *ibid.* **QE-11** (1975) 186.
8. M. S. DEMOKAN and P. A. LINDSAY, *Int. J. Electron.* **42** (1977) 417.
9. G. H. C. NEW, *Proc. IEEE* **67** (1979) 380.
10. W. H. LOWDERMILK, in "Laser Handbook", Vol. III, edited by M. L. Stitch (North Holland, Amsterdam, 1979) Chap. B1, p. 361.
11. J. HERRMANN and F. WEIDNER, *Opt. Quant. Electron.* **11** (1979) 119.
12. J. HERRMANN, F. WEIDNER and B. WILHELMI, *Appl. Phys.* **20** (1979) 237.
13. C. KOLMEDER and W. ZINTH, *ibid.* **24** (1981) 341.
14. G. H. C. NEW, *Rep. Prog. Phys.* **46** (1983) 877.
15. H. A. HAUS, *J. Appl. Phys.* **46** (1975) 3049.
16. M. S. DEMOKAN, "Mode-Locking in Solid-State and Semi-conductor Lasers" (Research Studies Press, Chichester, 1982).

17. A. LEITNER, M. E. LIPPITSCH, E. ROSCHGER and F. R. AUSSENEGG, *IEEE J. Quantum Electron.* **QE-19** (1983) 562.
18. J. HERRMANN and B. WILHELMI, "Laser für ultrakurze Lichtimpulse" (Physik Verlag, Weinheim, 1984).
19. A. PENZKOFER and N. WEINHARDT, in "Picosecond Phenomena III", Springer Series in Chemical Physics Vol. 23, edited by K. B. Eisenthal, R. M. Hochstrasser, W. Kaiser, and A. Laubereau (Springer, Berlin, 1982) p. 36.
20. *Idem, IEEE J. Quant. Electron.* **QE-19** (1982) 567.
21. F. SHIMIZU, *Phys. Rev. Lett.* **19** (1967) 1097.
22. T. K. GUSTAFSON, J. P. TARAN, H. A. HAUS, J. R. LIFSHITZ and P. L. KELLY, *Phys. Rev.* **177** (1969) 306.
23. V. V. KOROBKIN, A. A. MALYUTIN and A. M. PROKHOROV, *JETP Lett.* **12** (1970) 150.
24. S. A. AKHMANOV, R. V. KHOKHLOV and A. P. SUKHORUKOV, in "Laser Handbook", Vol. 2, edited by F. T. Arrecchi and E. O. Schultz-Dubois (North-Holland, Amsterdam, 1972) Chap. E3, p. 1131.
25. R. C. ECKARDT, C. H. LEE and J. N. BRADFORD, *Opto-Electron.* **6** (1974) 67.
26. O. SVELTO, *Progr. Opt.* **12** (1974) 1.
27. L. MANDEL and E. WOLF, *Rev. Mod. Phys.* **37** (1965) 231.
28. A. A. GRÜTTER, H. P. WEBER and R. DÄNDLIKER, *Phys. Rev.* **185** (1969) 629.
29. R. J. GLAUBER, *ibid.* **131** (1963) 2766.
30. V. S. LETOKHOV, *Sov. Phys. JETP* **23** (1966) 506.
31. A. W. TUCKER, M. BIRNBAUM and C. L. FINCHER, *J. Appl. Phys.* **53** (1982) 161.
32. V. B. KRAVCHENKO and Yu. P. RUDNITSKII, *Sov. J. Quant. Electron.* **9** (1979) 399.
33. R. K. KAZARYAN, *ibid.* **12** (1982) 1147.
34. M. MICHON, *IEEE J. Quant. Electron.* **QE-2** (1966) 612.
35. P. C. MAGNANTE, *ibid.* **QE-8** (1972) 440.
36. Yu. P. RUDNITSKII, R. V. SMIRNOV and V. M. CHEMYAK, *Sov. J. Quant. Electron.* **6** (1976) 1107.
37. S. M. YAREMA and D. MILAM, *IEEE J. Quant. Electron.* **18** (1982) 1941.
38. A. A. MAK, D. S. PRILEZHAEV, V. A. SEREBRYAKOV and A. D. STARIKOV, *Opt. Spectrosc.* **33** (1972) 381.
39. J. HERRMANN, F. WEIDNER and B. WILHELMI, *Appl. Phys.* **B26** (1981) 197.
40. W. KOECHNER, "Solid-State Laser Engineering", Springer Series in Optical Sciences, Vol. 1 (Springer, Berlin, 1976) p. 84.
41. M. HERCHER, *Appl. Opt.* **6** (1967) 947.
42. A. PENZKOFER and W. BLAU, *Opt. Quant. Electron.* **15** (1983) 325.
43. F. GRAF, C. LÖW and A. PENZKOFER, *Opt. Commun.* **47** (1983) 329.
44. F. GRAF, G. PLEININGER and A. PENZKOFER, *Appl. Phys.* **B34** (1984) 123.
45. B. KOPAINSKY, W. KAISER and K. H. DREXHAGE, *Opt. Commun.* **32** (1980) 451.
46. F. GRAF and A. PENZKOFER, *ibid.* **51** (1981) 111.
47. C. JUNG, F. HOLLINGER and H. WEBER, Technical Digest of CLEO'84, 19–22 June, Anaheim, California, p. 116.
48. R. R. ALFANO, N. H. SCHILLER and G. A. REYNOLDS, *IEEE J. Quant. Electron.* **QE-17** (1981) 290.
49. A. PENZKOFER and W. KAISER, *Appl. Phys. Lett.* **21** (1972) 547.
50. A. PENZKOFER and W. FALKENSTEIN, *Opt. Quant. Electron.* **10** (1978) 399.
51. S. E. STOKOVSKI, "Glass Lasers", in CRC Handbook of Laser Science and Technology, Vol. 1, Lasers and Masers, edited by M. J. Weber (CRC Press, Boca Raton FL, 1982), p. 215.
52. J. M. PELLEGRINO, W. M. YEN and M. J. WEBER, *J. Appl. Phys.* **51** (1980) 6332.
53. S. A. BRAWER and M. J. WEBER, *Appl. Phys. Lett.* **35** (1979) 31.
54. V. I. NIKITIN, M. S. SOSKIN and A. I. KHIZHNYAK, *Sov. Techn. Phys. Lett.* **3** (1977) 5.
55. F. GRAF and A. PENZKOFER, *Opt. Quant. Electron.* **17** (1985) 53.
56. R. C. ECKARDT, J. N. BRADFORD and C. H. LEE, *Appl. Phys. Lett.* **19** (1971) 420.
57. D. VON DER LINDE, *IEEE J. Quant. Electron.* **QE-8** (1972) 328.
58. *Idem, Appl. Phys.* **2** (1973) 281.
59. A. B. MIRNOV and O. B. SHATBERASHVILI, *Sov. J. Quant. Electron.* **4** (1974) 805.
60. D. J. BRADLEY and W. SIBBETT, *Opt. Commun.* **9** (1973) 17.
61. W. ZINTH, A. LAUBEREAU and W. KAISER, *ibid.* **22** (1977) 161.
62. T. R. ROYT, *ibid.* **35** (1980) 271.
63. G. R. FLEMING, I. R. HARROWFIELD, A. E. W. KNIGHT, J. M. MORRIS, R. J. ROBBINS and G. W. ROBINSON, *ibid.* **20** (1977) 36.
64. E. B. TREACY, *Phys. Lett.* **28A** (1968) 34.
65. R. A. FISHER, P. L. KELLEY and T. K. GUSTAFSON, *Appl. Phys. Lett.* **14** (169) 140.
66. E. B. TREACY, *ibid.* **17**(1970) 14.
67. A. N. ZHERIKHIN, P. G. KRYUKOV, Yu. A. MATVEETS and S. W. CHEKALIN, *Sov. J. Quant. Electron.* **4** (1974) 525.
68. S. V. CHEKALIN, P. G. KRYUKOV, Yu. A. MATVEETS and O. B. SHATBERASHVILI, *Opto-Electron.* **6** (1974) 249.
69. R. R. CUBEDDU and O. SVELTO, *IEEE J. Quant. Electron.* **QE-5** (1969) 495.
70. F. DEMARTINI, C. H. TOWNES, T. K. GUSTAFSON and P. L. KELLEY, *Phys. Rev.* **164** (1967) 312.
71. A. LAUBERAU and D. VON DER LINDE, *Z. Naturforschung* **25a** (1970) 1626.

72. J. A. GIORDMAINE, M. A. DUGUAY and J. W. HANSEN, *IEEE J. Quant. Electron.* **QE-4** (1968) 252.
73. M. A. DUGUAY and J. W. HANSEN, *Appl. Phys. Lett.* **14** (1969) 14.
74. B. NIKOLAUS and D. GRISCHKOWSKY, *Appl. Phys. Lett.* **43** (1983) 228.
75. A. M. WEINER, J. G. FUJIMOTO and E. P. IPPEN, in "Ultrafast Phenomena IV", Springer Series in Chemical Physics 38, edited by D. H. Auston and K. B. Eisenthal (Springer, Berlin, 1984) p. 11.
76. R. CUBEDDU, R. POLLONI, C. A. SACCHI and O. SVELTO, *Phys. Rev.* **A2** (1970) 1955.
77. C. H. LIN and T. K. GUSTAFSON, *IEEE J. Quant. Electron.* **QE-8** (1972) 429.
78. H. NATHEL, D. M. GUTHALS and J. H. I. CLARK, Technical Digest of CLEO'84, 19–22 June, 1984, Anaheim, California, p. 182.
79. P. SPERBER and A. PENZKOFER, *Opt. Commun.* (1985) to be published.
80. R. C. ECKARDT, *IEEE J. Quant. Electron.* **QE-10** (1974) 48.
81. A. YARIV, "Quantum Electron", 2nd Edition (Wiley, New York, 1975) p. 502.
82. J. M. MARBURGER, *Prog. Quant. Electron.* **4** (1975) 35.
83. Schott data sheet for Nd-phosphate laser glass LG703.
84. F. GRAF, J. SCHMIDT and A. PENZKOFER, *Opt. Commun.* (1985) to be published.
85. A. PENZKOFER, F. HÄRTINGER and J. WIEDMANN, *Appl. Phys.* **B26** (1981) 239.
86. B. P. BOCZAR and M. R. TOPP, *Appl. Opt.* **22** (1983) 1611.
87. B. BAREIKA, A. PISKARSKAS, V. SINKYAVICHYUS and V. SIRUTKAITIS, *Sov. J. Quant. Electron.* **14** (1984) 407.